Reconfigurable Intelligent Surface as a Micro Base Station: A Novel Paradigm for Small Cell Networks

Jun Wang, *Graduate Student Member, IEEE*, Ying-Chang Liang, *Fellow, IEEE*, Yiyang Pei, *Senior Member, IEEE*, and Xuemin Shen, *Fellow, IEEE*

***Abstract*— Small cell networks (SCNs) have emerged as a promising solution to meet the demand for increasing data traffic for the sixth generation and beyond wireless networks. However, power consumption and two-tier interference issues are two bottlenecks that hinder further development. This paper proposes a novel reconfigurable intelligent surface (RIS)-based SCN in which an RIS serves multiple micro users as a small cell base station while assisting the macro user's transmission. Compared to the conventional SCNs, the RIS-based SCN can achieve significant power reduction. Meanwhile, the reflected signal can be regarded as a multipath component instead of interference to the macro user. We propose two transmission schemes and formulate the design of the phase shift matrix at the RIS and the beamforming vector at the macro base station as an optimization problem. The alternating optimization algorithm is developed to optimize the phase shift matrix and the beamforming vector to minimize the total power consumption under the user rate and phase shift constraints. Simulation results show that the total power consumption can be reduced significantly by deploying the RIS in the SCN when the number of reflective elements is sufficiently large.**

***Index Terms*— Reconfigurable intelligent surface, small cell networks, alternating optimization, time division multiple access, space division multiple access, power consumption minimization, successive convex approximation.**

Manuscript received 12 January 2022; revised 12 June 2022 and 22 September 2022; accepted 22 September 2022. Date of publication 10 October 2022; date of current version 11 April 2023. This work was supported in part by the National Natural Science Foundation of China under Grant U1801261; in part by the National Key Research and Development Program of China under Grant 2018YFB1801105; in part by the Key Areas of Research and Development Program of Guangdong Province, China, under Grant 2018B010114001; in part by the Science and Technology Development Fund, Macau SAR, under Grant 0009/2020/A1; in part by the Fundamental Research Funds for the Central Universities under Grant ZYGX2019Z022; in part by the Programme of Introducing Talents of Discipline to Universities under Grant B20064; and in part by the National Research Foundation, Singapore, under its the AI Singapore Programme under Grant AISG2-RP-2020-019. An earlier version of this paper was presented in part at the 2021 IEEE Globecom [DOI: 10.1109/GLOBECOM46510.2021.9685214]. The associate editor coordinating the review of this article and approving it for publication was Y. Liu. *(Corresponding author: Ying-Chang Liang.)*

Jun Wang is with the National Key Laboratory of Science and Technology on Communications, University of Electronic Science and Technology of China, Chengdu 611731, China (e-mail: junwang@std.uestc.edu.cn).

Ying-Chang Liang is with the Center for Intelligent Networking and Communications, University of Electronic Science and Technology of China, Chengdu 611731, China, and also with the Yangtze Delta Region Institute (Huzhou), University of Electronic Science and Technology of China, Huzhou 313001, China (e-mail: liangyc@ieee.org).

Yiyang Pei is with the Singapore Institute of Technology, Singapore 138683 (e-mail: yiyang.pei@singaporetech.edu.sg).

Xuemin Shen is with the Department of Electrical and Computer Engineering, University of Waterloo, Waterloo, ON N2L 3G1, Canada (e-mail: sshen@uwaterloo.ca).

Color versions of one or more figures in this article are available at https://doi.org/10.1109/TWC.2022.3211191.

Digital Object Identifier 10.1109/TWC.2022.3211191

I. Introduction

ACCORDING to a forecast published by the International Telecommunication Union, mobile data traffic will expand at a 55 percent annual rate from 2020 to 2030, reaching 607 exabytes (EB) in 2025 and 5016 EB in 2030 [2]. The small cell network (SCN) is considered as a promising solution to accommodate such enormous traffic. SCNs can achieve improved coverage of blind areas and reduce traffic burden in each cell by densely deploying self-organized, low-power, and low-cost micro base stations (mBSs) [3]. The reduced cell size and densification of network cells will reduce the number of users in each cell, and thus boost the bandwidth available to each user. In the meantime, the smaller cell size reduces the distance between the user and the mBS, which improves the users' channels [4]. However, there are two key challenges to the mass deployment of small cells. First, the deployment of small cells brings additional co-tier and cross-tier interference to the conventional macro base station (MBS) only networks, resulting in network performance degradation. Such interference is challenging to manage with due to the random deployment and the lack of macro-micro backhaul link [5]. It is critical to develop effective interference management techniques to control two-tier interference [6]. Second, dense deployment of mBSs leads to high energy consumption. It is critical to reduce the power consumption and cost of deploying the densified small cells out of economic and environmental considerations.

Existing research attempts to address the interference challenge in SCN from different dimensions, such as time division multiple access (TDMA) scheduling in the time domain [7], [8], orthogonal frequency-division multiple access (OFDMA) scheduling [9], fractional frequency reuse [10] in the frequency domain, interference alignment in the space domain [11], [12], and power control in the power domain [13]. Furthermore, a distributed interference management scheme from a multi-domain perspective was proposed in [14], in which OFDMA scheduling, interference alignment, TDMA scheduling, and power optimization were implemented. However, these research works mainly consider avoiding interference instead of harnessing it. An effective approach to address the power challenge is to put several base stations into sleep while maintaining the quality of service (QoS) of users [15], [16],

[17], [18]. It was demonstrated in [15] that with the sleep mode mechanism, the operational energy could be reduced 50 to 90 percent when the cell size is small and the traffic is light. However, the power reduction is negligible in micro and macro cells or for heavy traffic. A strategic sleeping mechanism for SCNs was proposed in [16]. The range-expanded small cells were used to cover the area of the sleeping small cells which are far from the MBS while the macro cell was used to serve the users from the sleeping cells close to it. It was shown that the proposed repulsive scheme could significantly reduce the power consumption of the network. A joint energy-saving and interference-coordination design problem was considered in [17], and a two-level online learning approach was utilized to obtain the most energy-efficient control actions. An energy-saving scheme with joint user association, clustering, and on/off strategies was proposed in [18]. Despite the development of power-saving approaches, SCNs continue to face a power bottleneck since active mBSs consumes much power due to the utilization of active components including the local oscillator, up-converter, and power amplifier.

The reconfigurable intelligent surface (RIS) has recently been proposed by the academic community as another viable technique for improving coverage [19], [20], [21], [22]. With low-cost and low-power reflective elements, the RIS can achieve real-time control of amplitude and phase changes to adapt to the dynamic requirements under diverse channel environments [23], [24], [25]. The RIS does not need to actively generate new signals but only passively reflects the incident signals, and thus the power-hungry active components are not required. The roles of small cell and RIS deployment for coverage enhancement was compared in [26]. It was shown that with sufficient small cells, the deployment of RIS can notably reduce the network cost while maintaining the same network coverage. Besides operating as a passive relay to assist traditional communication systems, the RIS can also transmit its information by reconfiguring its phase shifts [27], [28], [29], [30], [31], [32], [33]. Specifically, an RIS-based multiple-input multiple-output (MIMO) transmitter was proposed in [27], which consists of a single radio frequency (RF) emitter that provides a dedicated unmodulated RF signal and an RIS that carries out the modulation and beamforming. This novel RIS-based transmitter architecture is more energy-efficient than the conventional MIMO transmitter due to the use of single-RF and RIS. An RIS-based quadrature phase shift keying (QPSK) prototype system was implemented in [28], in which the phase modulation was achieved by electrically controlling the RIS phase shifts. Besides the dedicated signal source, RIS can also transmit its information by riding on the RF signals in the environment. This type of system is called a symbiotic radio (SR) network. The RIS-assisted MIMO SR network, the multiuser multiple-input single-output (MISO) SR network, and the RIS-assisted unmanned aerial vehicle SR network were investigated in [29], [30], and [31], respectively. It was demonstrated that not only did the RIS gain an opportunity to transmit its information, but that the primary transmissions could also be considerably improved.

Due to the transmission capability of the RIS, we propose an RIS-based SCN, in which an RIS is employed to replace the conventional mBS to serve multiple micro users in an SCN. In the proposed system, the MBS transmits the signal to the macro user, and the RIS transmits information received from the wired backhaul to micro users by embedding it over the incident MBS signals. Deploying the RIS instead of conventional mBSs can provide several benefits. First, as it passively reflects the incident signals, the RIS consumes less power than a conventional mBS, making it a more energy-efficient solution, especially for large-scale deployment. Second, since the RIS signal can be considered as a multi-path component, the transmission rates of macro users can be improved. In this way, it addresses the interference problem in traditional SCNs since the interference relationship is transformed into a mutualistic one. Finally, since it has a large number of reflective elements, the RIS can accommodate more users simultaneously than a conventional mBS, which usually has a limited number of antennas. In this paper, we propose two transmission schemes to support multi-user information transmission in the RIS-based SCN, namely, space division multiple access (SDMA) and time division multiple access (TDMA) schemes. This paper aims to minimize the total power consumption by jointly optimizing the phase shift matrix at the RIS and the beamforming vector at the MBS under the transmission rate and phase shift constraints. We develop alternating optimization algorithms to solve the optimization problems under two transmission schemes. The contributions of the paper are summarized as follows:

- To the best of the authors' knowledge, this is the first paper to propose the RIS-based SCN in which the RIS serves multiple micro users in the SCN. The proposed system can achieve lower power consumption, avoid interference to the macro user, and support more simultaneous micro users transmission, making it more appealing for massive small cell deployment.
- We propose two transmission schemes, SDMA, and TDMA schemes, to realize multi-user information transmission in the RIS-based SCN. We jointly design the phase shift matrix at the RIS and the beamforming vector at the MBS to minimize the total power consumption under the transmission rate and phase shift constraints. Two optimization problems are formulated under the two transmission schemes correspondingly.
- The formulated problems are non-convex since the optimization variables are coupled. We apply alternating optimization to solve the problems iteratively. Several optimization techniques, such as successive convex approximation (SCA), semi-definite programming (SDP) and Gaussian randomization procedure are used to address the problems.
- Simulation results show that the total power consumption can be reduced significantly by deploying the RIS in the SCN, which validates the superiority of the RIS-based SCN and the effectiveness of the proposed algorithms.

The rest of this paper is organized as follows. Section II first introduces the system model for the proposed RIS-based SCN and formulate the total power consumption minimization

problem for both SDMA and TDMA transmission schemes. The proposed algorithms are presented in Section III. In Section IV, the conventional SCN system is introduced as a benchmark transmission scheme. Section V shows the simulation results to verify the advantages of the RIS-based SCN over the conventional SCN and validate the effectiveness of proposed algorithms. Finally, Section VI concludes the paper.

Notations: For complex vector $\boldsymbol{v}$, $\boldsymbol{v}^H$, $\mathrm{Re}(\boldsymbol{v})$, $\boldsymbol{v}_i$ and $\mathrm{diag}(\boldsymbol{v})$ denote the conjugate transpose, the real part, the ith element and the diagonal matrix with its diagonal elements given by $\boldsymbol{v}$, respectively. $\boldsymbol{a}\otimes\boldsymbol{b}$ denotes the Kronecker product of vector $\boldsymbol{a}$ and $\boldsymbol{b}$. $\mathrm{vec}\boldsymbol{A}$ denotes the vectorization operation for matrix $\boldsymbol{A}$. $\mathrm{tr}(\boldsymbol{A})$ and $\mathrm{rank}(\boldsymbol{A})$ denote the trace and rank of the matrix $\boldsymbol{A}$, respectively. $\boldsymbol{A}^\star$ denotes the optimal value of variable $\boldsymbol{A}$. $\boldsymbol{A}[m,n]$ and $\boldsymbol{A}[m,:]$ denote the (m,n)th element and the mth row vector of matrix $\boldsymbol{A}$, respectively. $\boldsymbol{A}\succeq 0$ denotes that $\boldsymbol{A}$ is a semi-definite matrix. $\boldsymbol{I}_K\in\mathbb{R}^{K\times K}$ is the identify matrix. $\mathcal{CN}(\mu,\sigma^2)$ denotes the distribution of a circularly symmetric complex Gaussian (CSCG) random variable with mean μ and variance σ^2.

II. System Model For RIS-Based Small Cell Network

In this section, we present the system model for the RIS-based small cell network, including the system description and signal models for SDMA and TDMA schemes.

A. System Description

As shown in Fig. 1(a), we consider an RIS-based SCN in which an MBS achieves wide area coverage while multiple RISs are deployed to serve small cells. Suppose that different small cells utilize different resource blocks to transmit information, and thus there is no interference between them. The scenario is reduced to the system shown in Fig. 1(b). The MBS is equipped with a uniform linear array (ULA) with M antennas, and the RIS is equipped with a uniform rectangular array (UPA) with $N=N_h\times N_v$ reflective elements, where N_h and N_v denote the numbers of reflective elements along the horizontal and vertical axes of the RIS. The MBS serves a single-antenna macro user (denoted as user 0), and the RIS serves K single-antenna micro users (denoted as user $k, k=1,\ldots,K$).

The channels from the MBS to the RIS, from the RIS to the macro user, from the RIS to micro user k, from the MBS to the macro user, and from the MBS to micro user k are denoted by $\boldsymbol{L}\in\mathbb{C}^{N\times M},\boldsymbol{h}_0\in\mathbb{C}^{1\times N},\boldsymbol{h}_k\in\mathbb{C}^{1\times N},\boldsymbol{g}_0\in\mathbb{C}^{1\times M},\boldsymbol{g}_k\in\mathbb{C}^{1\times M}$, respectively. Similar to [20], [29], we consider a block flat-fading channel model in this paper.[1] The large-scale path loss is set as follows [34]:

$$\beta(d)[\mathrm{dB}]=\begin{cases}G_t+G_r-35.95-22\log_{10}(d), & \text{LoS},\\ G_t+G_r-33.05-36.7\log_{10}(d). & \text{NLoS}.\end{cases} \tag{1}$$

[1]To simplify the model, we consider flat fading channels. However, the proposed methodologies can be readily extended to the frequency selective fading channels where OFDM-based transmitter and receiver are used.

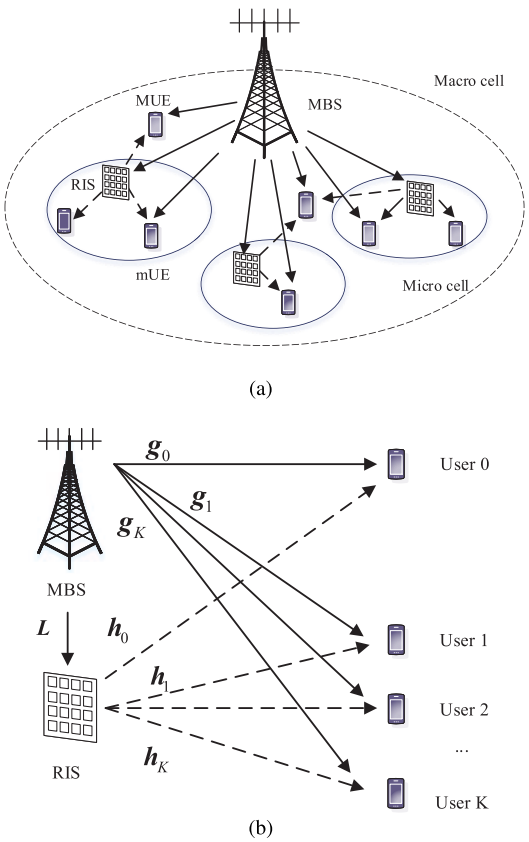

Fig. 1. (a) Application scenario for the RIS-based SCN; (b) The system model for RIS-based SCN, consisting of an MBS, an RIS, a macro user, and K micro users.

Here, G_t and G_r denote the antenna gains (in dBi) at the transmitter and receiver, respectively. The channels $\boldsymbol{L},\{\boldsymbol{h}_k\}_{k=1}^K$ are modeled as Rician channels while the channels $\boldsymbol{h}_0,\{\boldsymbol{g}_k\}_{k=0}^K$ are modeled as Rayleigh channels due to extensive scatters. In particular, the small-scale channel from the MBS to the RIS is denoted as

$$\widetilde{\boldsymbol{L}}=\sqrt{\frac{K_L}{1+K_L}}\boldsymbol{L}^{\mathrm{LoS}}+\sqrt{\frac{1}{1+K_L}}\boldsymbol{L}^{\mathrm{NLoS}}, \tag{2}$$

where K_L is the Rician factor for $\boldsymbol{L}$, $\boldsymbol{L}^{\mathrm{LoS}}$ is the deterministic line-of-sight (LoS) components, and $\boldsymbol{L}^{\mathrm{NLoS}}$ is the non-LoS components following the standard complex Gaussian distribution $\mathcal{CN}(0,1)$. The LoS component can be expressed by the steering vector model, given by

$$\boldsymbol{L}^{\mathrm{LoS}}=\boldsymbol{a}_R^H\left(\theta_{\mathrm{AoA,R}},\psi_{\mathrm{AoA,R}}\right)\boldsymbol{a}_B\left(\theta_{\mathrm{AoD,B}}\right), \tag{3}$$

where $\theta_{\mathrm{AoA,R}}$ and $\psi_{\mathrm{AoA,R}}$ denote the center azimuth angle of arrival (AoA) and elevation AoA, respectively, at the RIS, $\theta_{\mathrm{AoD,B}}$ denotes the angle of departure (AoD) at the MBS. The steering vectors can be further defined as

$$\begin{aligned}&\boldsymbol{a}_R^H\left(\theta_{\mathrm{AoA,R}},\psi_{\mathrm{AoA,R}}\right)\\&\quad=\boldsymbol{a}_v\left(\theta_{\mathrm{AoA,R}},\psi_{\mathrm{AoA,R}}\right)\otimes\boldsymbol{a}_h\left(\theta_{\mathrm{AoA,R}},\psi_{\mathrm{AoA,R}}\right)\\&\quad\in\mathbb{C}^{1\times N},\end{aligned} \tag{4}$$

$$\begin{aligned}&\boldsymbol{a}_B\left(\theta_{\mathrm{AoD,B}}\right)\\&\quad=\left[1,e^{-j\frac{2\pi d}{\lambda}\sin(\theta_{\mathrm{AoD,B}})},\ldots,e^{-j\frac{2\pi d}{\lambda}(M-1)\sin(\theta_{\mathrm{AoD,B}})}\right]\\&\quad\in\mathbb{C}^{1\times M},\end{aligned} \tag{5}$$

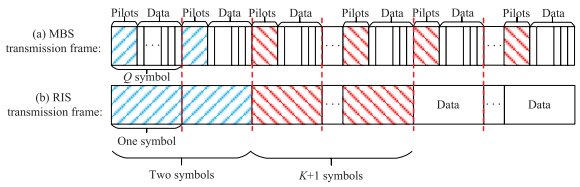

Fig. 2. The transmission frame structure of the RIS-based SCN. The blue shaded part denotes pilots for channel estimation. The MBS sends pilots while the RIS reflects the MBS signal with known phase shift matrices. The red shaded part denotes the pilots of the MBS and the RIS with the optimized beamforming vector and phase shift matrix.

where

$$[\boldsymbol{a}_h(\theta,\psi)]_n = e^{-j\frac{2\pi d}{\lambda}(n-1)\cos(\psi)\sin(\theta)}, \quad \forall n \in \{1,2,\ldots,N_h\}, \tag{6}$$

$$[\boldsymbol{a}_v(\theta,\psi)]_n = e^{j\frac{2\pi d}{\lambda}(n-1)\cos(\psi)\cos(\theta)}, \quad \forall n \in \{1,2,\ldots,N_v\}. \tag{7}$$

Here, d is the antenna element separation and λ is the wavelength. We set $d = \frac{1}{2}\lambda$ for simplicity. The small-scale path losses for other channels are similarly defined, and thus omitted.

Fig. 2 shows the transmission frame structure of the RIS-based SCN, which is a generalization of the one proposed in [29]. In the first two RIS symbols, the MBS sends pilots while the RIS reflects the MBS signal with known phase shift matrices for the macro and micro users to estimate the instantaneous CSI. The channels can be estimated by using the methods in [35], [36], [37], and [38]. After obtaining the CSI, the transmit beamforming vector and phase shift matrix can be optimized. In the following $K+1$ RIS symbols, the BS transmits with the optimized beamforming vector and the RIS reflects the MBS signal with the optimized phase shift. The users can then obtain the optimized beamforming vector and phase shift. After $K+3$ pilot symbols, the RIS starts to transmit data to the micro users. Similar to [29], we assume that the MBS sends pilots during each RIS symbol to eliminate the ambiguity between the MBS information and the RIS information when the direct link is blocked. Note that with the MBS pilots, the knowledge of the CSI as well as the optimized beamforming vector and phase shift matrix, the users can estimate the composited channel and decode their information accordingly.

The micro users can be served by the RIS simultaneously or one by one, and the corresponding transmission schemes are the SDMA and TDMA schemes, respectively. In the following, we present the signal models of these two transmission schemes.

B. Signal Model for SDMA Transmission Scheme

Under the SDMA transmission scheme, the RIS serves the micro users simultaneously. The MBS transmits the signal $s(q)$ with beamforming vector $\boldsymbol{w}_0 \in \mathbb{C}^{M\times 1}$ to the macro user, where $s(q)$ follows the distribution of $\mathcal{CN}(0,1)$. The RIS receives the signal from MBS, and then the information that needs to be sent to the K micro user is loaded onto the MBS signal by adjusting the phases of the reflection elements. The corresponding phase shift matrix for user k is denoted as $\boldsymbol{\Phi}_k = \text{diag}\{\theta_{k,1},\theta_{k,2},\ldots,\theta_{k,N}\} \in \mathbb{C}^{N\times N}$, where $\theta_{k,n}$ denotes the phase shift of the n-th element for user k. We assume that the RIS applies a phase shift keying (PSK) modulation scheme for information transmission. Denote c_k as the information that the RIS sends to user k. Similar to the conventional mBS, we assume c_k comes from the wired backhaul link. While designing the phase shift $\{\boldsymbol{\Phi}_k\}_{k=1}^K$, the overall phase shift matrix introduced by the RIS is given as $\boldsymbol{\Phi}(C) = \sum_{i=1}^K \boldsymbol{\Phi}_i c_i \in \mathbb{C}^{N\times N}$, where $C \triangleq \{c_1,c_2,\ldots,c_K\}$ is the symbol set for micro users. Denote the symbol period for the MBS and the RIS as T_s and T_c, respectively. It is assumed that $T_c = QT_s$, where Q is an integer.

The signal received by the macro user is written as

$$y_0(q) = \boldsymbol{g}_0\boldsymbol{w}_0 s(q) + \boldsymbol{h}_0\boldsymbol{\Phi}(C)\boldsymbol{L}\boldsymbol{w}_0 s(q) + u_0(q). \tag{8}$$

where the additive complex Gaussian noise $u_0(q)$ follows the distribution $\mathcal{CN}(0,\sigma_0^2)$.

The SNR at the macro user is given by

$$\gamma_0(C) = \frac{|\boldsymbol{g}_0\boldsymbol{w}_0 + \boldsymbol{h}_0\boldsymbol{\Phi}(C)\boldsymbol{L}\boldsymbol{w}_0|^2}{\sigma_0^2}. \tag{9}$$

The reflected signal from the RIS is no longer an interference to the macro user, but a multipath component, which leads to the increase in the SNR. In (9), the SNR contains C. Similar to [29], we assume that c_k changes fast compared with the channel variation. Therefore, the corresponding rate needs to take expectation over C, which is written as [29]

$$R_0 = \mathbb{E}_C\left(\log_2\left(1+\gamma_0(C)\right)\right). \tag{10}$$

According to Jensen's inequality, we have

$$R_0 \le \log_2\left(1+\mathbb{E}_C\left(\gamma_0(C)\right)\right). \tag{11}$$

Denote $m_i = \boldsymbol{h}_0\boldsymbol{\Phi}_i\boldsymbol{L}\boldsymbol{w}_0$ and $a = \boldsymbol{g}_0\boldsymbol{w}_0$. $\gamma_0(C)$ is rewritten as (12), shown at the bottom of the page.

Since $\mathbb{E}(c_k) = 0, \mathbb{E}(|c_k|^2) = 1, \forall k$, we take the expectation over C and obtain

$$\begin{aligned}\mathbb{E}_C\left(\gamma_0(C)\right) &= \frac{|a|^2 + \sum_{i=1}^K |m_i|^2}{\sigma_0^2} \\ &= \frac{\sum_{i=1}^K |\boldsymbol{h}_0\boldsymbol{\Phi}_i\boldsymbol{L}\boldsymbol{w}_0|^2 + |\boldsymbol{g}_0\boldsymbol{w}_0|^2}{\sigma_0^2}.\end{aligned} \tag{13}$$

$$\begin{aligned}\gamma_0(C) &= \frac{|a+\sum_{i=1}^K m_i c_i|^2}{\sigma_0^2} \\ &= \frac{|a|^2 + a^*\sum_{i=1}^K m_i c_i + a\sum_{j=1}^K m_j^* c_j^* + \sum_{i=1}^K\sum_{j=1}^K m_i c_i m_j^* c_j^*}{\sigma_0^2}.\end{aligned} \tag{12}$$

Hence, the upper bound of the achievable rate is given by

$$R_0 \leq \log_2\left(1+\frac{\sum_{i=1}^{K}|\boldsymbol{h}_0\boldsymbol{\Phi}_i\boldsymbol{L}\boldsymbol{w}_0|^2+|\boldsymbol{g}_0\boldsymbol{w}_0|^2}{\sigma_0^2}\right). \quad (14)$$

The signal received by user k is written as

$$y_k(q)=\boldsymbol{g}_k\boldsymbol{w}_0 s(q)+\boldsymbol{h}_k\sum_{i=1}^{K}\boldsymbol{\Phi}_i c_i\boldsymbol{L}\boldsymbol{w}_0 s(q)+u_k(q). \quad (15)$$

User k first decodes $s(q)$, performs successive interference cancellation (SIC) and then decodes c_k, similar to [39]. The upper bound of the achievable rate for user k to decode $s(q)$ is given by

$$R_{k,s}\leq \log_2\left(1+\frac{\sum_{i=1}^{K}|\boldsymbol{h}_k\boldsymbol{\Phi}_i\boldsymbol{L}\boldsymbol{w}_0|^2+|\boldsymbol{g}_k\boldsymbol{w}_0|^2}{\sigma_k^2}\right). \quad (16)$$

After decoding $s(q)$, the SIC technique is utilized to remove the direct link interference. Since the symbol period of c_k covers Q symbol period of $s(q)$, there are Q relatively independent paths for decoding c_k and maximal ratio combining (MRC) is applied to combine Q symbols of y_k. The signal-to-interference-plus-noise-ratio (SINR) for user k to decode c_k with MRC is written as

$$\gamma_{k,c_k}=\frac{|\boldsymbol{h}_k\boldsymbol{\Phi}_k\boldsymbol{L}\boldsymbol{w}_0|^2}{|\boldsymbol{h}_k\sum_{i=1,i\neq k}^{K}\boldsymbol{\Phi}_i\boldsymbol{L}\boldsymbol{w}_0|^2+\frac{\sigma_k^2}{Q}}. \quad (17)$$

The achievable rate for user k to decode c_k is given by

$$R_{k,c_k}=\frac{1}{Q}\log_2\left(1+\frac{|\boldsymbol{h}_k\boldsymbol{\Phi}_k\boldsymbol{L}\boldsymbol{w}_0|^2}{|\boldsymbol{h}_k\sum_{i=1,i\neq k}^{K}\boldsymbol{\Phi}_i\boldsymbol{L}\boldsymbol{w}_0|^2+\frac{\sigma_k^2}{Q}}\right). \quad (18)$$

The power consumption model of different types of BSs is given by [40]

$$P_{BS}=\lambda\left(\frac{P_S}{\eta}+MP_c\right), \quad (19)$$

where η is the power amplifier efficiency, P_S is the BS transmit power, M is the number of the transmit antennas, P_c is the circuit power consumption, and λ denotes the influence of cooling, direct current to direct current (DC-DC) and main supply. For different types of BSs, the exact values of η, P_c and λ can be different. The power consumption model of RIS is given by [41]

$$P_{RIS}=NP_n(b), \quad (20)$$

where N is the number of reflective elements, and $P_n(b)$ denotes the power consumption of each phase shifter with a resolution of b bits. The total power consumption of the proposed RIS-based SCN under SDMA transmission scheme is given by

$$P_{SDMA}=\lambda_1\left(\frac{1}{\eta_1}\|\boldsymbol{w}_0\|^2+MP_{c,MBS}\right)+NP_n(b). \quad (21)$$

Remark 1: The motivation of considering the total power consumption is as follows. By deploying the RIS instead of mBS, the consumed circuit power used to serve the micro users can be reduced. Meanwhile, the signal from the RIS is a multipath component to the macro user and the SNR seen by the macro user can be increased. Therefore, the transmit power consumption at the MBS can also be reduced. For the above two considerations, in order to have a holistic comparison from a system level, we consider the total power consumption in this paper.

C. Signal Model for TDMA Transmission Scheme

Under the TDMA transmission scheme, micro users are served one by one by the RIS. In each RIS symbol, only one micro user transmits, and thus we can design the beamforming vector and phase shift matrix for each user separately.[2] Denote the beamforming vector at the MBS and phase shift matrix at the RIS for user k as $\boldsymbol{w}_{0,k}\in\mathbb{C}^{M\times 1}$ and $\boldsymbol{\Phi}_k\in\mathbb{C}^{N\times N}$, respectively. The overall RIS phase shifts for user k is $\boldsymbol{\Phi}_k c_k$. The received signal at the macro user is given by

$$y_0(q)=\boldsymbol{g}_0\boldsymbol{w}_{0,k}s(q)+\boldsymbol{h}_0\boldsymbol{\Phi}_k c_k\boldsymbol{L}\boldsymbol{w}_{0,k}s(q)+u_0(q). \quad (22)$$

The resulting SNR is given by

$$\gamma_0(c_k)=\frac{|\boldsymbol{g}_0\boldsymbol{w}_{0,k}+\boldsymbol{h}_0\boldsymbol{\Phi}_k c_k\boldsymbol{L}\boldsymbol{w}_{0,k}|^2}{\sigma_0^2}. \quad (23)$$

The corresponding rate needs to take expectation over c_k, which is written as

$$R_0=\mathbb{E}_{c_k}\left(\log_2\left(1+\gamma_0(c_k)\right)\right). \quad (24)$$

According to Jensen's inequality, we have

$$R_0\leq\log_2\left(1+\mathbb{E}_{c_k}\left(\gamma_0(c_k)\right)\right), \quad (25)$$

where

$$\begin{aligned}\mathbb{E}_{c_k}\left(\gamma_0(c_k)\right)&=\mathbb{E}_{c_k}\left(\frac{|\boldsymbol{g}_0\boldsymbol{w}_{0,k}+\boldsymbol{h}_0\boldsymbol{\Phi}_k c_k\boldsymbol{L}\boldsymbol{w}_{0,k}|^2}{\sigma_0^2}\right)\\&=\frac{|\boldsymbol{g}_0\boldsymbol{w}_{0,k}|^2+|\boldsymbol{h}_0\boldsymbol{\Phi}_k\boldsymbol{L}\boldsymbol{w}_{0,k}|^2}{\sigma_0^2}.\end{aligned} \quad (26)$$

Hence, the achievable rate of the macro user is upper-bounded by

$$R_0\leq\log_2\left(1+\frac{|\boldsymbol{g}_0\boldsymbol{w}_{0,k}|^2+|\boldsymbol{h}_0\boldsymbol{\Phi}_k\boldsymbol{L}\boldsymbol{w}_{0,k}|^2}{\sigma_0^2}\right). \quad (27)$$

The received signal at user k during its transmission slot is given by

$$\begin{aligned}y_k(q)=\boldsymbol{g}_k\boldsymbol{w}_{0,k}s(q)+\boldsymbol{h}_k\boldsymbol{\Phi}_k c_k\boldsymbol{L}\boldsymbol{w}_{0,k}s(q)+u_k(q),\\ q=(k-1)Q+1,\ldots,kQ.\end{aligned} \quad (28)$$

User k first decodes $s(q)$, performs SIC, and then decodes c_k. The SNR for micro user k to decode $s(q)$ is written as

$$\gamma_{k,s}(c_k)=\frac{|\boldsymbol{g}_k\boldsymbol{w}_{0,k}+\boldsymbol{h}_k\boldsymbol{\Phi}_k c_k\boldsymbol{L}\boldsymbol{w}_{0,k}|^2}{\sigma_k^2}. \quad (29)$$

Then the upper bound of the achievable rate of user k is given by

$$R_{k,s}\leq\log_2\left(1+\frac{|\boldsymbol{g}_k\boldsymbol{w}_{0,k}|^2+|\boldsymbol{h}_k\boldsymbol{\Phi}_k\boldsymbol{L}\boldsymbol{w}_{0,k}|^2}{\sigma_k^2}\right). \quad (30)$$

[2]Alternatively, we can use the same beamforming vector at the MBS for all micro users while optimizing the phase shift matrix individually. However, such a design is inferior to our considered scheme.

Similarly, since the symbol period of c_k covers Q symbol periods of $s(q)$, by applying MRC, the SNR for user k to decode c_k is written as

$$\gamma_{k,c_k} = \frac{Q|\boldsymbol{h}_k \boldsymbol{\Phi}_k \boldsymbol{L} \boldsymbol{w}_{0,k}|^2}{\sigma_k^2}. \tag{31}$$

The corresponding rate is given by

$$R_{k,c_k} = \frac{1}{Q}\log_2\left(1 + \frac{Q|\boldsymbol{h}_k \boldsymbol{\Phi}_k \boldsymbol{L} \boldsymbol{w}_{0,k}|^2}{\sigma_k^2}\right). \tag{32}$$

The total power consumption of the proposed RIS-based SCN under the TDMA transmission mode is given by

$$P_{TDMA} = \lambda_1 \left(\frac{\sum_{k=1}^{K} \|\boldsymbol{w}_{0,k}\|^2}{\eta_1 K} + M P_{c,MBS}\right) + N P_n(b). \tag{33}$$

D. Problem Formulation

This paper aims to minimize the total power consumption by jointly optimizing the beamforming vector at the MBS and phase shift matrix at the RIS, subject to the user transmission rate constraints and RIS phase shift constraints.[3]

1) SDMA Transmission Scheme: Note that circuit power is fixed while the transmit power can be controlled by designing the beamforming vectors. The total power consumption minimization problem is reduced to the transmit power minimization problem. Mathematically, the optimization problem can be formulated as

$$(\mathbf{P}-\mathbf{S}): \min_{\{\boldsymbol{\Phi}_k\}_{k=1}^K, \boldsymbol{w}_0} \|\boldsymbol{w}_0\|^2 \tag{34a}$$

$$\text{s.t. } R_0 \geq \bar{R}_s, \tag{34b}$$

$$R_{k,s} \geq \bar{R}_s, \quad \forall k, \tag{34c}$$

$$R_{k,c_k} \geq \bar{R}_c, \quad \forall k, \tag{34d}$$

$$|\boldsymbol{\Phi}(C)[n,n]| \leq 1, \quad \forall n, \ \forall C. \tag{34e}$$

where $\bar{R}_s$ and $\bar{R}_c$ denote the desired transmission rate of the macro user and micro users. (34b) denotes the macro user transmission rate constraint. (34c) and (34d) ensure that both $s(q)$ and c_k can be decoded successfully at micro users. The constraint (34e) indicates that the phase shift constraints should be met for all combinations of $\{c_i\}_{i=1}^K$.

2) TDMA Transmission Scheme: The total power consumption minimization problem can be tackled separately for different micro users since the subproblems for different micro users are independent. For user k, the problem is reduced to the transmit power minimization problem, formulated as

$$(\mathbf{P}-\mathbf{T}): \min_{\boldsymbol{\Phi}_k, \boldsymbol{w}_{0,k}} \|\boldsymbol{w}_{0,k}\|^2 \tag{35a}$$

$$\text{s.t. } R_0 \geq \bar{R}_s, \tag{35b}$$

$$R_{k,s} \geq \bar{R}_s, \tag{35c}$$

$$\frac{1}{K} R_{k,c_k} \geq \bar{R}_c, \tag{35d}$$

$$|\boldsymbol{\Phi}_k[n,n]| \leq 1, \quad \forall n, \tag{35e}$$

Similar to Problem $(\mathbf{P}-\mathbf{S})$, (35b), (35c), (35d), and (35e) represent the macro user rate constraint, micro user rate constraints, and phase shift constraints, respectively. Note that the factor $\frac{1}{K}$ in (35d) is due to the TDMA time-sharing principle since each user can only transmit once every K time slots.

The optimization variables $\{\boldsymbol{\Phi}_k\}_{k=1}^K$ and $\boldsymbol{w}_0$ are coupled in problem $(\mathbf{P}-\mathbf{S})$ and $(\mathbf{P}-\mathbf{T})$ and cannot be tackled separately, resulting in non-convex optimization problems. In the following, we will transform the problems into a more tractable form.

III. Proposed Algorithms

A. Proposed Algorithm for SDMA Transmission Scheme

Since the optimization variables $\{\boldsymbol{\Phi}_k\}_{k=1}^K$ and $\boldsymbol{w}_0$ are coupled in the constraints, we apply alternating optimization to optimize them alternatively [20].

1) Beamforming Optimization: For given $\{\boldsymbol{\Phi}_k\}_{k=1}^K$, the beamforming vector $\boldsymbol{w}_0$ can be optimized by solving the subproblem as follows:

$$(\mathbf{P}-\mathbf{S1}): \min_{\boldsymbol{w}_0} \|\boldsymbol{w}_0\|^2 \quad \text{s.t. (34b), (34c) and (34d).} \tag{36}$$

The subproblem can be transformed into

$$(\mathbf{P}-\mathbf{S2}):$$

$$\min_{\boldsymbol{w}_0} \text{tr}\left(\boldsymbol{w}_0 \boldsymbol{w}_0^H\right) \tag{37a}$$

$$\text{s.t. } \frac{|\boldsymbol{h}_k \boldsymbol{\Phi}_k \boldsymbol{L} \boldsymbol{w}_0|^2}{|\boldsymbol{h}_k \sum_{i=1, i\neq k}^K \boldsymbol{\Phi}_i \boldsymbol{L} \boldsymbol{w}_0|^2 + \frac{\sigma_k^2}{Q}} \geq 2^{Q\bar{R}_c} - 1, \quad \forall k, \tag{37b}$$

$$\frac{\sum_{i=1}^K |\boldsymbol{h}_0 \boldsymbol{\Phi}_i \boldsymbol{L} \boldsymbol{w}_0|^2 + |\boldsymbol{g}_0 \boldsymbol{w}_0|^2}{\sigma_0^2} \geq 2^{\bar{R}_s} - 1, \tag{37c}$$

$$\frac{\sum_{i=1}^K |\boldsymbol{h}_k \boldsymbol{\Phi}_i \boldsymbol{L} \boldsymbol{w}_0|^2 + |\boldsymbol{g}_k \boldsymbol{w}_0|^2}{\sigma_k^2} \geq 2^{\bar{R}_s} - 1, \quad \forall k. \tag{37d}$$

By denoting $\boldsymbol{W}_0 = \boldsymbol{w}_0 \boldsymbol{w}_0^H$, the problem $(\mathbf{P}-\mathbf{S2})$ can be recast as

$$(\mathbf{P}-\mathbf{S3}): \min_{\boldsymbol{W}_0} \text{tr}\left(\boldsymbol{W}_0\right) \tag{38a}$$

$$\text{s.t. } \text{tr}(\boldsymbol{J}_k \boldsymbol{W}_0) - (2^{Q\bar{R}_c} - 1)\text{tr}(\boldsymbol{M}_k \boldsymbol{W}_0) \geq (2^{Q\bar{R}_c} - 1)\frac{\sigma_k^2}{Q}, \quad \forall k, \tag{38b}$$

$$\text{tr}(\boldsymbol{V}_0 \boldsymbol{W}_0) \geq (2^{\bar{R}_s} - 1)\sigma_0^2, \tag{38c}$$

$$\text{tr}(\boldsymbol{V}_k \boldsymbol{W}_0) \geq (2^{\bar{R}_s} - 1)\sigma_k^2, \forall k, \tag{38d}$$

$$\boldsymbol{W}_0 \succeq 0, \tag{38e}$$

$$\text{rank}(\boldsymbol{W}_0) = 1, \tag{38f}$$

where

$$\boldsymbol{J}_k = \boldsymbol{L}^H \boldsymbol{\Phi}_k^H \boldsymbol{h}_k^H \boldsymbol{h}_k \boldsymbol{\Phi}_k \boldsymbol{L}, \tag{39}$$

[3]We consider the ideal reflection model in this paper, in which the reflection phase and amplitude can be adjusted independently. The ideal model can be extended to the practical model similar to existing works [42], [43]. Note that the performance by assuming the ideal model can serve as an upper bound of the performance that the practical model can achieve. The RIS phase shift design considering practical model in the proposed RIS-based SCN system is worth further investigation.

$$\boldsymbol{M}_k = \boldsymbol{L}^H \sum_{i=1,i\neq k}^{K} \boldsymbol{\Phi}_i^H \boldsymbol{h}_k^H \boldsymbol{h}_k \sum_{i=1,i\neq k}^{K} \boldsymbol{\Phi}_i \boldsymbol{L}, \tag{40}$$

$$\boldsymbol{V}_0 = \sum_{i=1}^{K} \boldsymbol{L}^H \boldsymbol{\Phi}_i^H \boldsymbol{h}_0^H \boldsymbol{h}_0 \boldsymbol{\Phi}_i \boldsymbol{L} + \boldsymbol{g}_0^H \boldsymbol{g}_0, \tag{41}$$

$$\boldsymbol{V}_k = \sum_{i=1}^{K} \boldsymbol{L}^H \boldsymbol{\Phi}_i^H \boldsymbol{h}_k^H \boldsymbol{h}_k \boldsymbol{\Phi}_i \boldsymbol{L} + \boldsymbol{g}_k^H \boldsymbol{g}_k. \tag{42}$$

We solve the problem $(\mathbf{P}-\mathbf{S3})$ with the SDR technique. Specifically, the rank constraint (38f) is first relaxed and a solution to the rank-relaxed optimization problem is obtained with CVX [44]. Gaussian randomization procedure is then performed to obtain a rank-one solution [45].

2) Phase Shift Optimization: For a given $\boldsymbol{W}_0$, the phase shift $\{\boldsymbol{\Phi}_k\}_{k=1}^K$ can be optimized by solving the subproblem as follows:

$$(\mathbf{P}-\mathbf{S4}): \text{ find } \{\boldsymbol{\Phi}_k\}_{k=1}^K \quad \text{s.t. (34b), (34c), (34d) and (34e).} \tag{43}$$

Denote $\boldsymbol{\phi}_k = (\theta_{k,1}, \theta_{k,2}, \ldots, \theta_{k,N}) \in \mathbb{C}^{1\times N}, \boldsymbol{c} = (c_1, c_2, \ldots, c_K) \in \mathbb{C}^{1\times K}$. By letting

$$\boldsymbol{\Psi} = \begin{pmatrix} \theta_{1,1} & \theta_{1,2} & \ldots & \theta_{1,N} \\ \theta_{2,1} & \theta_{2,2} & \ldots & \theta_{2,N} \\ \ldots & \ldots & \ldots & \ldots \\ \theta_{K,1} & \theta_{K,2} & \ldots & \theta_{K,N} \end{pmatrix} = \begin{pmatrix} \boldsymbol{\phi}_1 \\ \boldsymbol{\phi}_2 \\ \ldots \\ \boldsymbol{\phi}_K \end{pmatrix} \in \mathbb{C}^{K\times N}, \tag{44}$$

the constraint (34e) can be rewritten as

$$|\boldsymbol{c}\boldsymbol{\Psi}\boldsymbol{e}_n| \leq 1, \quad \forall n, \boldsymbol{c}, \tag{45}$$

where $\boldsymbol{e}_n$ is the canonical vector, in which the n-th element is 1 while other elements are 0. Meanwhile, we can obtain

$$\begin{aligned} \boldsymbol{h}_k \boldsymbol{\Phi}_k \boldsymbol{L}\boldsymbol{w}_0 &= \boldsymbol{\phi}_k \text{diag}(\boldsymbol{h}_k)\boldsymbol{L}\boldsymbol{w}_0 \\ &= \boldsymbol{e}_k^H \boldsymbol{\Psi} \text{diag}(\boldsymbol{h}_k)\boldsymbol{L}\boldsymbol{w}_0, \end{aligned} \tag{46}$$

$$\begin{aligned} \boldsymbol{h}_k \sum_{i=1,i\neq k}^{K} \boldsymbol{\Phi}_i \boldsymbol{L}\boldsymbol{w}_0 &= \sum_{i=1,i\neq k}^{K} \boldsymbol{\phi}_i \text{diag}(\boldsymbol{h}_k)\boldsymbol{L}\boldsymbol{w}_0 \\ &= (\mathbf{1} - \boldsymbol{e}_k^H)\boldsymbol{\Psi}\text{diag}(\boldsymbol{h}_k)\boldsymbol{L}\boldsymbol{w}_0. \end{aligned} \tag{47}$$

The problem $(\mathbf{P}-\mathbf{S4})$ can be transformed into

$(\mathbf{P}-\mathbf{S5})$:

$$\text{find } \boldsymbol{\Psi} \tag{48a}$$

$$\text{s.t. } \frac{|\boldsymbol{e}_k^H \boldsymbol{\Psi}\text{diag}(\boldsymbol{h}_k)\boldsymbol{L}\boldsymbol{w}_0|^2}{|(\mathbf{1}-\boldsymbol{e}_k^H)\boldsymbol{\Psi}\text{diag}(\boldsymbol{h}_k)\boldsymbol{L}\boldsymbol{w}_0|^2 + \frac{\sigma_k^2}{Q}} \geq 2^{Q\bar{R}_c} - 1, \quad \forall k, \tag{48b}$$

$$\frac{\sum_{i=1}^{K} |\boldsymbol{e}_i^H \boldsymbol{\Psi}\text{diag}(\boldsymbol{h}_0)\boldsymbol{L}\boldsymbol{w}_0|^2 + |\boldsymbol{g}_0\boldsymbol{w}_0|^2}{\sigma_0^2} \geq 2^{\bar{R}_s} - 1, \tag{48c}$$

$$\frac{\sum_{i=1}^{K} |\boldsymbol{e}_i^H \boldsymbol{\Psi}\text{diag}(\boldsymbol{h}_k)\boldsymbol{L}\boldsymbol{w}_0|^2 + |\boldsymbol{g}_k\boldsymbol{w}_0|^2}{\sigma_k^2} \geq 2^{\bar{R}_s} - 1, \quad \forall k, \tag{48d}$$

$$|\boldsymbol{c}\boldsymbol{\Psi}\boldsymbol{e}_n| \leq 1, \quad \forall n, \boldsymbol{c}. \tag{48e}$$

We can rewrite the numerator in (48b) as

$$\begin{aligned} &|\boldsymbol{e}_k^H \boldsymbol{\Psi}\text{diag}(\boldsymbol{h}_k)\boldsymbol{L}\boldsymbol{w}_0|^2 \\ &= \text{tr}\left(\boldsymbol{\Psi}^H \boldsymbol{e}_k \boldsymbol{e}_k^H \boldsymbol{\Psi}\text{diag}(\boldsymbol{h}_k)\boldsymbol{L}\boldsymbol{w}_0 \boldsymbol{w}_0^H \boldsymbol{L}^H \text{diag}(\boldsymbol{h}_k)^H\right) \\ &= (\text{vec}\boldsymbol{\Psi})^H \text{vec}\left(\boldsymbol{e}_k \boldsymbol{e}_k^H \boldsymbol{\Psi}\text{diag}(\boldsymbol{h}_k)\boldsymbol{L}\boldsymbol{w}_0 \boldsymbol{w}_0^H \boldsymbol{L}^H \text{diag}(\boldsymbol{h}_k)^H\right) \\ &= (\text{vec}\boldsymbol{\Psi})^H \left(\left(\text{diag}(\boldsymbol{h}_k)\boldsymbol{L}\boldsymbol{w}_0 \boldsymbol{w}_0^H \boldsymbol{L}^H \text{diag}(\boldsymbol{h}_k)^H\right)^T \otimes \boldsymbol{e}_k \boldsymbol{e}_k^H\right) \\ &\quad \times \text{vec}\boldsymbol{\Psi} \\ &= (\text{vec}\boldsymbol{\Psi})^H \left(\left(\text{diag}(\boldsymbol{h}_k)\boldsymbol{L}\boldsymbol{W}_0 \boldsymbol{L}^H \text{diag}(\boldsymbol{h}_k)^H\right)^T \otimes \boldsymbol{e}_k \boldsymbol{e}_k^H\right) \\ &\quad \times \text{vec}\boldsymbol{\Psi} \\ &\triangleq \boldsymbol{v}^H \boldsymbol{E}_k \boldsymbol{v}, \end{aligned} \tag{49}$$

where $\boldsymbol{E}_k = \left(\text{diag}(\boldsymbol{h}_k)\boldsymbol{L}\boldsymbol{W}_0 \boldsymbol{L}^H \text{diag}(\boldsymbol{h}_k)^H\right)^T \otimes \boldsymbol{e}_k \boldsymbol{e}_k^H$ and $\boldsymbol{v} = \text{vec}\boldsymbol{\Psi}$. Similarly, for the first item of the denominator in (48b), we have

$$|(\mathbf{1}-\boldsymbol{e}_k^H)\boldsymbol{\Psi}\text{diag}(\boldsymbol{h}_k)\boldsymbol{L}\boldsymbol{w}_0|^2 \triangleq \boldsymbol{v}^H \boldsymbol{F}_k \boldsymbol{v}, \tag{50}$$

where $\boldsymbol{F}_k = \left(\text{diag}(\boldsymbol{h}_k)\boldsymbol{L}\boldsymbol{W}_0 \boldsymbol{L}^H \text{diag}(\boldsymbol{h}_k)^H\right)^T \otimes (\mathbf{1} - \boldsymbol{e}_k^H)^H(\mathbf{1}-\boldsymbol{e}_k^H)$.

For (48c), (48d) and (48e), we have

$$\sum_{i=1}^{K} |\boldsymbol{e}_i^H \boldsymbol{\Psi}\text{diag}(\boldsymbol{h}_0)\boldsymbol{L}\boldsymbol{w}_0|^2 \triangleq \boldsymbol{v}^H \boldsymbol{G}_0 \boldsymbol{v}, \tag{51}$$

$$\sum_{i=1}^{K} |\boldsymbol{e}_i^H \boldsymbol{\Psi}\text{diag}(\boldsymbol{h}_k)\boldsymbol{L}\boldsymbol{w}_0|^2 \triangleq \boldsymbol{v}^H \boldsymbol{G}_k \boldsymbol{v}, \tag{52}$$

$$|\boldsymbol{c}\boldsymbol{\Psi}\boldsymbol{e}_n|^2 = \boldsymbol{v}^H \left((\boldsymbol{e}_n \boldsymbol{e}_n^H)^T \otimes \boldsymbol{c}^H \boldsymbol{c}\right) \boldsymbol{v}, \tag{53}$$

where $\boldsymbol{G}_0 = \left(\text{diag}(\boldsymbol{h}_0)\boldsymbol{L}\boldsymbol{W}_0 \boldsymbol{L}^H \text{diag}(\boldsymbol{h}_0)^H\right)^T \otimes \boldsymbol{I}_K, \boldsymbol{G}_k = \left(\text{diag}(\boldsymbol{h}_k)\boldsymbol{L}\boldsymbol{W}_0 \boldsymbol{L}^H \text{diag}(\boldsymbol{h}_k)^H\right)^T \otimes \boldsymbol{I}_K$. By integrating (49), (50), (51), (52) and (53), the problem $(\mathbf{P}-\mathbf{S5})$ can be rewritten as the following problem:

$(\mathbf{P}-\mathbf{S6})$:

$$\text{find } \boldsymbol{v} \tag{54a}$$

$$\text{s.t. } \boldsymbol{v}^H \boldsymbol{E}_k \boldsymbol{v} \geq \left(2^{Q\bar{R}_c} - 1\right)\left(\boldsymbol{v}^H \boldsymbol{F}_k \boldsymbol{v} + \frac{\sigma_k^2}{Q}\right), \quad \forall k, \tag{54b}$$

$$\boldsymbol{v}^H \boldsymbol{G}_0 \boldsymbol{v} + |\boldsymbol{g}_0\boldsymbol{w}_0|^2 \geq \left(2^{\bar{R}_s} - 1\right)\sigma_0^2, \tag{54c}$$

$$\boldsymbol{v}^H \boldsymbol{G}_k \boldsymbol{v} + |\boldsymbol{g}_k\boldsymbol{w}_0|^2 \geq \left(2^{\bar{R}_s} - 1\right)\sigma_k^2, \quad \forall k, \tag{54d}$$

$$\boldsymbol{v}^H \left((\boldsymbol{e}_n \boldsymbol{e}_n^H)^T \otimes \boldsymbol{c}^H \boldsymbol{c}\right) \boldsymbol{v} \leq 1, \quad \forall n, \boldsymbol{c}. \tag{54e}$$

Since $\boldsymbol{E}_k$, $\boldsymbol{G}_0$ and $\boldsymbol{G}_k$ are semi-definite matrices, we can apply the SCA approach to tackle the non-convex constraints. Specifically, for (54b) we will apply the first order expansion to $\boldsymbol{v}^H \boldsymbol{E}_k \boldsymbol{v}$ at a given point $\boldsymbol{v}_t$, resulting in the following inequality

$$\boldsymbol{v}^H \boldsymbol{E}_k \boldsymbol{v} \geq 2\text{Re}\left(\boldsymbol{v}_t^H \boldsymbol{E}_k \boldsymbol{v}\right) - \boldsymbol{v}_t^H \boldsymbol{E}_k \boldsymbol{v}_t. \tag{55}$$

We can tackle (54c) and (54d) in a similar way. Hence, the problem $(\mathbf{P}-\mathbf{S6})$ can be further transformed into

$$
\begin{aligned}
&(\mathbf{P}-\mathbf{S7}):\\
&\quad \text{find } \boldsymbol{v} && (56a)\\
&\quad \text{s.t. } 2\text{Re}\left(\boldsymbol{v}_t^H\boldsymbol{E}_k\boldsymbol{v}\right)-\boldsymbol{v}_t^H\boldsymbol{E}_k\boldsymbol{v}_t\\
&\qquad \geq \left(2^{Q\bar{R}_c}-1\right)\left(\boldsymbol{v}^H\boldsymbol{F}_k\boldsymbol{v}+\frac{\sigma_k^2}{Q}\right),\quad \forall k, && (56b)\\
&\qquad 2\text{Re}\left(\boldsymbol{v}_t^H\boldsymbol{G}_0\boldsymbol{v}\right)-\boldsymbol{v}_t^H\boldsymbol{G}_0\boldsymbol{v}_t+|\boldsymbol{g}_0\boldsymbol{w}_0|^2\\
&\qquad \geq \left(2^{\bar{R}_s}-1\right)\sigma_0^2, && (56c)\\
&\qquad 2\text{Re}\left(\boldsymbol{v}^H\boldsymbol{G}_k\boldsymbol{v}\right)-\boldsymbol{v}_t^H\boldsymbol{G}_k\boldsymbol{v}_t+|\boldsymbol{g}_k\boldsymbol{w}_0|^2\\
&\qquad \geq \left(2^{\bar{R}_s}-1\right)\sigma_k^2,\quad \forall k, && (56d)\\
&\qquad \boldsymbol{v}^H\left((\boldsymbol{e}_n\boldsymbol{e}_n^H)^T\otimes\boldsymbol{c}^H\boldsymbol{c}\right)\boldsymbol{v}\leq 1,\quad \forall n,\boldsymbol{c}. && (56e)
\end{aligned}
$$

We then introduce the rate residuals $\{\alpha_k\}_{k=1}^K$ and $\{\delta_k\}_{k=1}^{K+1}$ to transform the feasibility problem $(\mathbf{P}-\mathbf{S7})$ into a rate residuals maximization problem, written as:

$$
\begin{aligned}
&(\mathbf{P}-\mathbf{S8}):\\
&\max_{\{\alpha_k\}_{k=1}^K,\{\delta_k\}_{k=1}^{K+1},\boldsymbol{v}} \sum_{k=1}^{K}\alpha_k+\sum_{k=1}^{K+1}\delta_k && (57a)\\
&\quad \text{s.t. } 2\text{Re}\left(\boldsymbol{v}_t^H\boldsymbol{E}_k\boldsymbol{v}\right)-\boldsymbol{v}_t^H\boldsymbol{E}_k\boldsymbol{v}_t\\
&\qquad \geq \left(2^{Q\bar{R}_c}-1\right)\left(\boldsymbol{v}^H\boldsymbol{F}_k\boldsymbol{v}+\frac{\sigma_k^2}{Q}\right)+\alpha_k,\quad \forall k, && (57b)\\
&\qquad 2\text{Re}\left(\boldsymbol{v}^H\boldsymbol{G}_k\boldsymbol{v}\right)-\boldsymbol{v}_t^H\boldsymbol{G}_k\boldsymbol{v}_t+|\boldsymbol{g}_k\boldsymbol{w}_0|^2\\
&\qquad \geq \left(2^{\bar{R}_s}-1\right)\sigma_k^2+\delta_k,\quad \forall k, && (57c)\\
&\qquad 2\text{Re}\left(\boldsymbol{v}_t^H\boldsymbol{G}_0\boldsymbol{v}\right)-\boldsymbol{v}_t^H\boldsymbol{G}_0\boldsymbol{v}_t+|\boldsymbol{g}_0\boldsymbol{w}_0|^2\\
&\qquad \geq \left(2^{\bar{R}_s}-1\right)\sigma_0^2+\delta_{K+1}, && (57d)\\
&\qquad \boldsymbol{v}^H\left((\boldsymbol{e}_n\boldsymbol{e}_n^H)^T\otimes\boldsymbol{c}^H\boldsymbol{c}\right)\boldsymbol{v}\leq 1,\quad \forall n,\boldsymbol{c}, && (57e)\\
&\qquad \alpha_k\geq 0,\quad \delta_k\geq 0,\quad \forall k. && (57f)
\end{aligned}
$$

The problem $(\mathbf{P}-\mathbf{S8})$ is convex with respect to $\boldsymbol{v}$ and can be solved with CVX. The detailed steps are summarized in Algorithm 1.

Remark 2: The motivation for introducing the rate residuals is as follows. The problem $(\mathbf{P}-\mathbf{S7})$ is a feasibility problem and there may be multiple feasible solutions. If $(\mathbf{P}-\mathbf{S7})$ is solved, we may end up with a feasible but low-quality solution. By introducing the rate residuals, the solution of $(\mathbf{P}-\mathbf{S8})$ can always ensure that the achieved rate is higher than the rate requirement, which leaves room for further improvement of W_0 in the next iteration.

B. Proposed Algorithm for TDMA Transmission Scheme

The problem $(\mathbf{P}-\mathbf{T})$ can be written explicitly as

$$
\begin{aligned}
&(\mathbf{P}-\mathbf{T1}):\\
&\min_{\boldsymbol{\Phi}_k,\boldsymbol{w}_{0,k}} \|\boldsymbol{w}_{0,k}\|^2 && (58a)\\
&\quad \text{s.t. } \log_2\left(1+\frac{|\boldsymbol{g}_0\boldsymbol{w}_{0,k}|^2+|\boldsymbol{h}_0\boldsymbol{\Phi}_k\boldsymbol{L}\boldsymbol{w}_{0,k}|^2}{\sigma_0^2}\right)\\
&\qquad \geq \bar{R}_s, && (58b)\\
&\qquad \log_2\left(1+\frac{|\boldsymbol{g}_k\boldsymbol{w}_{0,k}|^2+|\boldsymbol{h}_k\boldsymbol{\Phi}_k\boldsymbol{L}\boldsymbol{w}_{0,k}|^2}{\sigma_k^2}\right)\\
&\qquad \geq \bar{R}_s, && (58c)\\
&\qquad \frac{1}{Q}\log\left(1+\frac{Q|\boldsymbol{h}_k\boldsymbol{\Phi}_k\boldsymbol{L}\boldsymbol{w}_{0,k}|^2}{\sigma_k^2}\right)\geq K\bar{R}_c, && (58d)\\
&\qquad |\boldsymbol{\Phi}_k[n,n]|\leq 1,\quad \forall n. && (58e)
\end{aligned}
$$

The optimization variables $\boldsymbol{\Phi}_k$ and $\boldsymbol{w}_{0,k}$ are coupled in the problem $(\mathbf{P}-\mathbf{T1})$. We split the problem into two subproblems and solve them with alternating optimization. The beamforming matrix and phase shifts are optimized in each subproblem with the other one is fixed, respectively.

1) Beamforming Optimization: For given $\boldsymbol{\Phi}_k$, the subproblem is written as

$$
\begin{aligned}
&(\mathbf{P}-\mathbf{T2}):\ \min_{\boldsymbol{w}_{0,k}} \|\boldsymbol{w}_{0,k}\|^2 && (59a)\\
&\quad \text{s.t. } |\boldsymbol{g}_0\boldsymbol{w}_{0,k}|^2+|\boldsymbol{h}_0\boldsymbol{\Phi}_k\boldsymbol{L}\boldsymbol{w}_{0,k}|^2\\
&\qquad \geq \left(2^{\bar{R}_s}-1\right)\sigma_0^2, && (59b)\\
&\qquad |\boldsymbol{g}_k\boldsymbol{w}_{0,k}|^2+|\boldsymbol{h}_k\boldsymbol{\Phi}_k\boldsymbol{L}\boldsymbol{w}_{0,k}|^2\\
&\qquad \geq \left(2^{\bar{R}_s}-1\right)\sigma_k^2, && (59c)\\
&\qquad Q|\boldsymbol{h}_k\boldsymbol{\Phi}_k\boldsymbol{L}\boldsymbol{w}_{0,k}|^2\geq\left(2^{QK\bar{R}_c}-1\right)\sigma_k^2. && (59d)
\end{aligned}
$$

The problem can be transformed into

$$
\begin{aligned}
&(\mathbf{P}-\mathbf{T3}):\\
&\min_{\boldsymbol{w}_{0,k}} \text{tr}\left(\boldsymbol{w}_{0,k}\boldsymbol{w}_{0,k}^H\right) && (60a)\\
&\quad \text{s.t. } \text{tr}\left(\boldsymbol{w}_{0,k}\boldsymbol{w}_{0,k}^H\left(\boldsymbol{g}_0^H\boldsymbol{g}_0+\boldsymbol{\Xi}_{0,k}\right)\right)\\
&\qquad \geq \left(2^{\bar{R}_s}-1\right)\sigma_0^2, && (60b)
\end{aligned}
$$

Algorithm 1 Proposed Algorithm to Solve $(\mathbf{P}-\mathbf{S})$

1: Initialize $\left\{\boldsymbol{\Phi}_k^{(0)}\right\}_{k=1}^K$, $\boldsymbol{w}_0^{(0)}$ and ϵ (a relatively small positive value).
2: Compute $\boldsymbol{v}^{(0)}$ and $\boldsymbol{W}_0^{(0)}$.
3: Let $t=0$.
4: **repeat**
5: Solve $(\mathbf{P}-\mathbf{S3})$ for given $\left\{\boldsymbol{\Phi}_k^{(t)}\right\}_{k=1}^K$, and obtain the optimal solution as $\boldsymbol{W}_0^{(t+1)}$.
6: Solve $(\mathbf{P}-\mathbf{S8})$ for given $\boldsymbol{W}_0^{(t+1)}$ with $\boldsymbol{v}_t=\boldsymbol{v}^{(t)}$, and obtain the optimal solution as $\boldsymbol{v}^{(t+1)}$.
7: Compute $\left\{\boldsymbol{\Phi}_k^{(t+1)}\right\}_{k=1}^K$ with $\boldsymbol{v}^{(t+1)}$.
8: Update iteration index $t=t+1$.
9: **until** $\text{tr}\left(\boldsymbol{W}_0^{(t)}-\boldsymbol{W}_0^{(t-1)}\right)\leq\epsilon$.
10: Obtain the optimal solution $\boldsymbol{W}_0^\star=\boldsymbol{W}_0^{(t)}$, and $\boldsymbol{v}^\star=\boldsymbol{v}^{(t)}$.
11: Recover $\{\boldsymbol{\Phi}_k^\star\}_{k=1}^K$ with $\boldsymbol{v}^\star$.
12: Perform Gaussian randomization procedure for $\boldsymbol{W}_0^\star$ and obtain the optimal $\boldsymbol{w}_0^\star$ [45].
13: Return the optimal solution $\boldsymbol{w}_0^\star$ and $\{\boldsymbol{\Phi}_k^\star\}_{k=1}^K$.

$$\text{tr}\left(\boldsymbol{w}_{0,k}\boldsymbol{w}_{0,k}^H\left(\boldsymbol{g}_k^H\boldsymbol{g}_k+\boldsymbol{\Xi}_{k,k}\right)\right) \geq \left(2^{\bar{R}_s}-1\right)\sigma_0^2, \tag{60c}$$

$$Q\text{tr}\left(\boldsymbol{w}_{0,k}\boldsymbol{w}_{0,k}^H\boldsymbol{\Xi}_{k,k}\right) \geq \left(2^{QK\bar{R}_c}-1\right)\sigma_k^2, \tag{60d}$$

where $\boldsymbol{\Xi}_{0,k} = \boldsymbol{L}^H\boldsymbol{\Phi}_k^H\boldsymbol{h}_0^H\boldsymbol{h}_0\boldsymbol{\Phi}_k\boldsymbol{L}$, $\boldsymbol{\Xi}_{k,k} = \boldsymbol{L}^H\boldsymbol{\Phi}_k^H\boldsymbol{h}_k^H\boldsymbol{h}_k\boldsymbol{\Phi}_k\boldsymbol{L}$. Denote $\boldsymbol{W}_{0,k} = \boldsymbol{w}_{0,k}\boldsymbol{w}_{0,k}^H$, the problem $(\mathbf{P}-\mathbf{T3})$ can be recast as

$$(\mathbf{P}-\mathbf{T4}):$$

$$\min_{\boldsymbol{W}_{0,k}} \text{tr}\left(\boldsymbol{W}_{0,k}\right) \tag{61a}$$

$$\text{s.t. tr}\left(\boldsymbol{W}_{0,k}\left(\boldsymbol{g}_0^H\boldsymbol{g}_0+\boldsymbol{\Xi}_{0,k}\right)\right) \geq \left(2^{\bar{R}_s}-1\right)\sigma_0^2, \tag{61b}$$

$$\text{tr}\left(\boldsymbol{W}_{0,k}\left(\boldsymbol{g}_k^H\boldsymbol{g}_k+\boldsymbol{\Xi}_{k,k}\right)\right) \geq \left(2^{\bar{R}_s}-1\right)\sigma_k^2, \tag{61c}$$

$$Q\text{tr}\left(\boldsymbol{W}_{0,k}\boldsymbol{\Xi}_{k,k}\right) \geq \left(2^{QK\bar{R}_c}-1\right)\sigma_k^2, \tag{61d}$$

$$\boldsymbol{W}_{0,k} \succeq 0, \tag{61e}$$

$$\text{rank}\left(\boldsymbol{W}_{0,k}\right) = 1. \tag{61f}$$

The problem $(\mathbf{P}-\mathbf{T4})$ can be solved by using the SDR technique, similar to problem $(\mathbf{P}-\mathbf{S3})$.

2) Phase Shift Optimization: For given $\boldsymbol{w}_{0,k}$, the subproblem to optimize $\boldsymbol{\Phi}_k$ is given by

$$(\mathbf{P}-\mathbf{T5}): \text{ find } \boldsymbol{\Phi}_k \quad \text{s.t. (35b), (35c), (35d) and (35e).} \tag{62}$$

Denote $\boldsymbol{\Upsilon}_k = \phi_k^H\phi_k$, the problem $(\mathbf{P}-\mathbf{T5})$ can be transformed into

$$(\mathbf{P}-\mathbf{T6}):$$

$$\text{find } \boldsymbol{\Upsilon}_k \tag{63a}$$

$$\text{s.t. tr}\left(\boldsymbol{\Upsilon}_k\text{diag}\left(\boldsymbol{h}_0\right)\boldsymbol{L}\boldsymbol{W}_{0,k}\boldsymbol{L}^H\text{diag}\left(\boldsymbol{h}_0\right)^H\right) \geq \left(2^{\bar{R}_s}-1\right)\sigma_0^2 - \text{tr}\left(\boldsymbol{g}_0^H\boldsymbol{g}_0\boldsymbol{W}_{0,k}\right), \tag{63b}$$

$$\text{tr}\left(\boldsymbol{\Upsilon}_k\text{diag}\left(\boldsymbol{h}_k\right)\boldsymbol{L}\boldsymbol{W}_{0,k}\boldsymbol{L}^H\text{diag}\left(\boldsymbol{h}_k\right)^H\right) \geq \left(2^{\bar{R}_s}-1\right)\sigma_k^2 - \text{tr}\left(\boldsymbol{g}_k^H\boldsymbol{g}_k\boldsymbol{W}_{0,k}\right), \tag{63c}$$

$$Q\text{tr}\left(\boldsymbol{\Upsilon}_k\text{diag}\left(\boldsymbol{h}_k\right)\boldsymbol{L}\boldsymbol{W}_{0,k}\boldsymbol{L}^H\text{diag}\left(\boldsymbol{h}_k\right)^H\right) \geq \left(2^{QK\bar{R}_c}-1\right)\sigma_k^2, \tag{63d}$$

$$\boldsymbol{\Upsilon}_k[n,n] \leq 1, \quad \forall n, \tag{63e}$$

$$\text{rank}(\boldsymbol{\Upsilon}_k) = 1, \tag{63f}$$

$$\boldsymbol{\Upsilon}_k \succeq 0. \tag{63g}$$

The problem $(\mathbf{P}-\mathbf{T6})$ is a feasibility problem. Similarly, by introducing rate residual variables $\{\beta_k\}_{k=1}^3$ and dropping the rank-one constraint, the problem can be recast as:

$$(\mathbf{P}-\mathbf{T7}):$$

$$\max_{\{\beta_k\}_{k=1}^3,\boldsymbol{\Upsilon}_k} \sum_{k=1}^3\beta_k \tag{64a}$$

$$\text{s.t. tr}\left(\boldsymbol{\Upsilon}_k\text{diag}\left(\boldsymbol{h}_0\right)\boldsymbol{L}\boldsymbol{W}_{0,k}\boldsymbol{L}^H\text{diag}\left(\boldsymbol{h}_0\right)^H\right) \geq \left(2^{\bar{R}_s}-1\right)\sigma_0^2 - \text{tr}\left(\boldsymbol{g}_0^H\boldsymbol{g}_0\boldsymbol{W}_{0,k}\right)+\beta_1, \tag{64b}$$

Algorithm 2 Proposed Algorithm to Solve $(\mathbf{P}-\mathbf{T})$

1: Initialize $\boldsymbol{\Phi}_k^{(0)}$, $\boldsymbol{w}_{0,k}^{(0)}$ and ϵ (a relatively small positive value).
2: Compute $\boldsymbol{\Upsilon}_k^{(0)}$ and $\boldsymbol{W}^{(0)}$.
3: Let $t=0$.
4: **repeat**
5: Solve $(\mathbf{P}-\mathbf{T4})$ for given $\boldsymbol{\Upsilon}_k^{(t)}$, and obtain the optimal solution as $\boldsymbol{W}_{0,k}^{(t+1)}$.
6: Solve $(\mathbf{P}-\mathbf{T7})$ for given $\boldsymbol{W}_{0,k}^{(t+1)}$, and obtain the optimal solution as $\boldsymbol{\Upsilon}_k^{(t+1)}$.
7: Update iteration index $t=t+1$.
8: **until** $\text{tr}\left(\boldsymbol{W}_{0,k}^{(t)}-\boldsymbol{W}_{0,k}^{(t-1)}\right) \leq \epsilon$.
9: Obtain the optimal solution $\boldsymbol{W}_{0,k}^\star = \boldsymbol{W}_{0,k}^{(t+1)}$, and $\boldsymbol{\Upsilon}_k^\star = \boldsymbol{\Upsilon}_k^{(t)}$.
10: Perform the Gaussian randomization procedure for $\boldsymbol{W}_{0,k}^\star$ and $\boldsymbol{\Upsilon}_k^\star$, and obtain the optimal $\boldsymbol{w}_{0,k}^\star$ and $\boldsymbol{\Phi}_k^\star$.
11: Return the optimal solution $\boldsymbol{w}_{0,k}^\star$ and $\boldsymbol{\Phi}_k^\star$.

$$\text{tr}\left(\boldsymbol{\Upsilon}_k\text{diag}\left(\boldsymbol{h}_k\right)\boldsymbol{L}\boldsymbol{W}_{0,k}\boldsymbol{L}^H\text{diag}\left(\boldsymbol{h}_k\right)^H\right) \geq \left(2^{\bar{R}_s}-1\right)\sigma_k^2 - \text{tr}\left(\boldsymbol{g}_k^H\boldsymbol{g}_k\boldsymbol{W}_{0,k}\right)+\beta_2, \tag{64c}$$

$$Q\text{tr}\left(\boldsymbol{\Upsilon}_k\text{diag}\left(\boldsymbol{h}_k\right)\boldsymbol{L}\boldsymbol{W}_{0,k}\boldsymbol{L}^H\text{diag}\left(\boldsymbol{h}_k\right)^H\right) \geq \left(2^{QK\bar{R}_c}-1\right)\sigma_k^2+\beta_3, \quad (63e) \text{ and } (63g). \tag{64d}$$

The problem $(\mathbf{P}-\mathbf{T7})$ is an SDP problem that can be solved directly. We note that $\boldsymbol{\Upsilon}_k$ and $\boldsymbol{W}_{0,k}$ are alternatively solved during each iteration. To reduce the computational complexity, Gaussian randomization procedure is performed to obtain the rank-one solution after the convergence of the alternating optimization. The overall algorithm is summarized in Algorithm 2.

C. Convergence and Complexity Analysis

1) Convergence Analysis: The convergence performance of the proposed algorithms is presented in Theorem 1.

Theorem 1: Algorithm 1 generates a sequence $\left\{\left(\boldsymbol{W}_0^{(t)},\boldsymbol{v}^{(t)}\right)\right\}$ of improved points of problem $(\mathbf{P}-\mathbf{S})$, which converges to a Karush-Kuhn-Tucker (KKT) point.

Proof: For algorithm 1, We have the following inequalities:

$$P\left(\boldsymbol{W}_0^{(t-1)},\boldsymbol{v}^{(t-1)}\right) \overset{(a)}{=} P\left(\boldsymbol{W}_0^{(t-1)},\boldsymbol{v}^{(t)}\right) \overset{(b)}{\geq} P\left(\boldsymbol{W}_0^{(t)},\boldsymbol{v}^{(t)}\right). \tag{65}$$

The inequality (a) holds since the transmit power only depends on $\boldsymbol{W}_0$ while the inequality (b) holds since $\boldsymbol{W}_0^{(t)}$ is the optimal solution of $(\mathbf{P}-\mathbf{S3})$ for given $\boldsymbol{v}^{(t)}$. Therefore, $\left\{\left(\boldsymbol{W}_0^{(t)},\boldsymbol{v}^{(t)}\right)\right\}$ is a better solution to problem $(\mathbf{P}-\mathbf{S})$ than $\left\{\left(\boldsymbol{W}_0^{(t-1)},\boldsymbol{v}^{(t-1)}\right)\right\}$. Furthermore, the

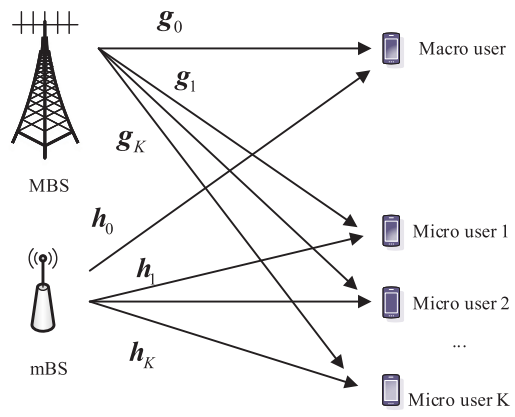

Fig. 3. The system model for conventional SCN, consisting of an MBS, an mBS, a macro user and K micro users.

sequence $\left\{\left(\boldsymbol{W}_0^{(t)}, \boldsymbol{v}^{(t)}\right)\right\}$ is bounded by the constraint (34e) and due to the fact that the objective function is to minimize $\mathrm{tr}\,(\boldsymbol{W}_0)$. According to Cauchy's theorem, there is a convergent subsequence $\left\{\left(\boldsymbol{W}_0^{(t_v)}, \boldsymbol{v}^{(t_v)}\right)\right\}$ with a limit point $(\boldsymbol{W}_0^\star, \boldsymbol{v}^\star)$. Following the proposition 2 in [46], we can obtain that

$$\lim_{t\to\infty}\left[P\left(\boldsymbol{W}_0^{(t)}, \boldsymbol{v}^{(t)}\right) - P\left(\boldsymbol{W}_0^\star, \boldsymbol{v}^\star\right)\right] = 0. \tag{66}$$

Notice that $\boldsymbol{W}_0^\star$ and $\boldsymbol{v}^\star$ are the optimal solutions of the convex optimization problems $(\mathbf{P}-\mathbf{S3})$ and $(\mathbf{P}-\mathbf{S8})$, respectively. According to [47], each accumulation point $(\boldsymbol{W}_0^\star, \boldsymbol{v}^\star)$ of the sequence $\left(\boldsymbol{W}_0^{(t)}, \boldsymbol{v}^{(t)}\right)$ is a KKT point. ■

The convergence proof of algorithm 2 is similar and is thus omitted here.

2) Complexity Analysis: The computational complexity of the proposed algorithms is analyzed in this part. According to [45], the computational complexity for solving $(\mathbf{P}-\mathbf{S3})$ is $\mathcal{O}\left(\max\{2K+1, M\}^4 M^{\frac{1}{2}}\log(\frac{1}{\epsilon_s})\right)$, where ϵ_s denotes the predefined accuracy of the solution. For solving $(\mathbf{P}-\mathbf{S8})$, the complexity is $\mathcal{O}\left((2^K N+2K+1)^4(KN+2K+1)^{\frac{1}{2}}\log(\frac{1}{\epsilon_s})\right)$. The complexity of randomization procedure is $\mathcal{O}\left(N^2\right)$. Let I_s and I_a denote the required iteration number for the SCA approach and the alternating optimization algorithm, respectively. Therefore, the total computational complexity of algorithm 1 is $\mathcal{O}\Big(I_a(\max\{2K+1, M\}^4 M^{\frac{1}{2}} + I_s(2^K N + 2K + 1)^4(KN+2K+1)^{\frac{1}{2}})\log(\frac{1}{\epsilon_s}) + N^2\Big)$. Similarly, the computational complexity for solving $(\mathbf{P}-\mathbf{T4})$ is $\mathcal{O}\left(M^2\log(\frac{1}{\epsilon_s})\right)$ while the complexity is $\mathcal{O}\left((N+3)^4 M^{\frac{1}{2}}\log(\frac{1}{\epsilon_s})\right)$ for solving $(\mathbf{P}-\mathbf{T7})$. The total computational complexity of algorithm 2 is $\mathcal{O}\left(I_a\left((N+3)^4 M^{\frac{1}{2}} + M^2\right)\log(\frac{1}{\epsilon_s}) + N^2\right)$.

IV. Conventional SCN

In this section, we review the conventional SCN as a benchmark transmission scheme. As illustrated in Fig. 3, the conventional SCN consists of an MBS with M_1 antennas, an mBS with M_2 antennas, a single-antenna macro user served by the MBS, and K single-antenna micro users served by the mBS. The baseband equivalent channels from the MBS to the macro user, from the MBS to micro user k, from the mBS to the macro user, and from the mBS to micro user k are denoted by $\boldsymbol{g}_0 \in \mathbb{C}^{1\times M_1}, \boldsymbol{g}_k \in \mathbb{C}^{1\times M_1}, \boldsymbol{h}_0 \in \mathbb{C}^{1\times M_2}, \boldsymbol{h}_k \in \mathbb{C}^{1\times M_2}$, respectively. The MBS transmits the signal $s(q)$ to the macro user with beamforming vector $\boldsymbol{w}_0 \in \mathbb{C}^{M_1\times 1}$ and the mBS transmits the signal $c_k(q), k = 1, \ldots, K$ to K micro users with beamforming vector $\boldsymbol{w}_k \in \mathbb{C}^{M_2\times 1}$. It is assumed that $s(q)$ and $c_k(q)$ follow the distribution of $\mathcal{CN}(0,1)$ and $c_k(q)$ comes from the wired backhaul. The signal received by the macro user is given by

$$y_0(q) = \boldsymbol{g}_0\boldsymbol{w}_0 s(q) + \boldsymbol{h}_0\sum_{i=1}^K \boldsymbol{w}_i c_i(q) + u_0(q), \tag{67}$$

where $u_0(q)$ is the additive white Gaussian noise at the macro user with zero mean and variance σ_0^2. The rate for macro user decoding $s(q)$ is given by

$$R_0 = \log_2\left(1 + \frac{|\boldsymbol{g}_0\boldsymbol{w}_0|^2}{\sum_{i=1}^K |\boldsymbol{h}_0\boldsymbol{w}_i|^2 + \sigma_0^2}\right). \tag{68}$$

For micro user k, its received signal is given by

$$y_k(q) = \boldsymbol{g}_k\boldsymbol{w}_0 s(q) + \boldsymbol{h}_k\sum_{i=1}^K \boldsymbol{w}_i c_i(q) + u_k(q), \tag{69}$$

where $u_k(q)$ is additive white Gaussian noise at user k following $\mathcal{CN}(0,\sigma_k^2)$. The micro user k first decodes $s(q)$. The corresponding rate is written as

$$R_{k,s} = \log_2\left(1 + \frac{|\boldsymbol{g}_k\boldsymbol{w}_0|^2}{\sum_{i=1}^K |\boldsymbol{h}_k\boldsymbol{w}_i|^2 + \sigma_k^2}\right). \tag{70}$$

After decoding $s(q)$, user k cancels the interference and then decodes $c_k(q)$. The rate to decode $c_k(q)$ is given by

$$R_{k,c} = \log_2\left(1 + \frac{|\boldsymbol{h}_k\boldsymbol{w}_k|^2}{\sum_{i=1,i\neq k}^K |\boldsymbol{h}_k\boldsymbol{w}_i|^2 + \sigma_k^2}\right). \tag{71}$$

The total power consumption in this SCN consists of the power consumed by both the MBS and mBS, which is given by

$$P_{all} = \lambda_1\left(\frac{1}{\eta_1}\|\boldsymbol{w}_0\|^2 + M_1 P_{c,MBS}\right) + \lambda_2\left(\frac{1}{\eta_2}\sum_{i=1}^K \|\boldsymbol{w}_i\|^2 + M_2 P_{c,mBS}\right), \tag{72}$$

where λ_1 and η_1 are the corresponding parameters for MBS while λ_2 and η_2 are those for mBS.

To minimize the total power consumption in SCN under user transmission rate constraints, the following problem can be formulated:

$$(\mathbf{P}-\mathbf{C}): \min_{\{\boldsymbol{w}_i\}_{i=0}^K} \frac{\lambda_1}{\eta_1}\|\boldsymbol{w}_0\|^2 + \frac{\lambda_2}{\eta_2}\sum_{i=1}^K \|\boldsymbol{w}_i\|^2 \tag{73a}$$

$$\text{s.t. } R_0 \geq \bar{R}_s, \tag{73b}$$

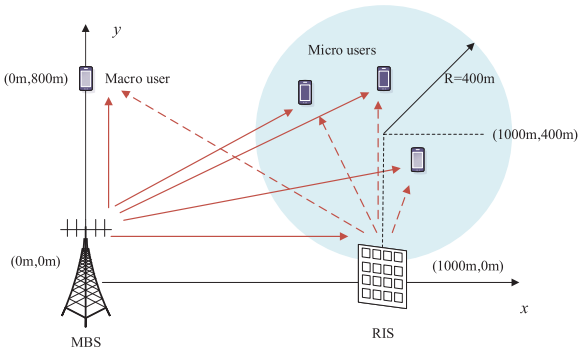

Fig. 4. The simulated RIS-based SCN comprising of one MBS, one N-element RIS, multiple micro users and one macro user.

$$R_{k,s} \geq \bar{R}_s, \quad \forall k, \tag{73c}$$

$$R_{k,c} \geq \bar{R}_c, \quad \forall k. \tag{73d}$$

Such a problem can be transformed to a rank-constrained SDP problem and solved with semi-definite relaxation (SDR) approach [45].

V. Simulation Results

In this section, simulation results are presented to validate the benefits of using an RIS to serve multiple micro users in an SCN. In the simulations, as shown in Fig. 7, the MBS is located at (0 m, 0 m), and the RIS is located at (1000 m, 0 m). The micro users are uniformly and randomly distributed in a circle centered at (1000 m, 400 m) with radius $R = 400$ m. The macro user is located at (0 m, 800 m). $N = 64$ ($N_h = 16, N_v = 4$). We assume that the RIS and the MBS have a gain of 5 dBi, and users have a gain of 0 dBi. The Rician factors for all Rician fading channels are set to 10.

We assume that the RIS applies binary phase shift keying (BPSK) modulation, i.e., $c_k = \{+1, -1\}$. The symbol period of the RIS is ten times longer than that of the MBS, i.e. $Q = 10$. The operating frequency is set to 2.5 GHz. The bandwidth is $B = 180$ kHz and the noise power is set to be $\sigma^2 = -174 + 10\log_{10}(B)$ dBm. The parameters in the power consumption model for MBS and mBS are set to $\lambda_1 = 1.25$, $\eta_1 = 0.388$, $P_{c,MBS} = 20.7$ W, $\lambda_2 = 1.15$, $\eta_2 = 0.285$, $P_{c,mBS} = 14.4$ W, which are identical to those in [40]. The power consumption value of each phase shifter is 7.8 mW for a 6-bit resolution phase shifting. Simulation results are averaged over 10^3 random channel realizations.

First, we study the convergence performance of the two transmission schemes, which are depicted in Fig. 5 and Fig. 6, respectively. For both algorithms, the transmit power under various $\bar{R}_s$ values decreases monotonically as the number of iterations increases. Furthermore, the proposed algorithms converge in three iterations for the TDMA scheme and 9 to 10 iterations for the SDMA scheme, which validates that the proposed algorithms can achieve fast convergence. A few iterations are sufficient to achieve a large portion of the converged transmit power, demonstrating the proposed algorithms' effectiveness and potential to be applied in practical scenarios.

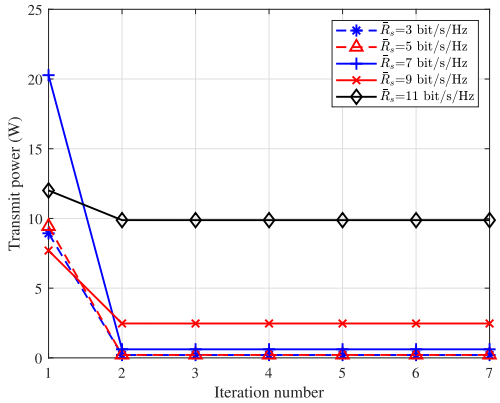

Fig. 5. Transmit power vs. Iteration number for TDMA transmission scheme, $K = 2, M = 3, M_2 = 2, \bar{R}_c = 0.2$ bit/s/Hz.

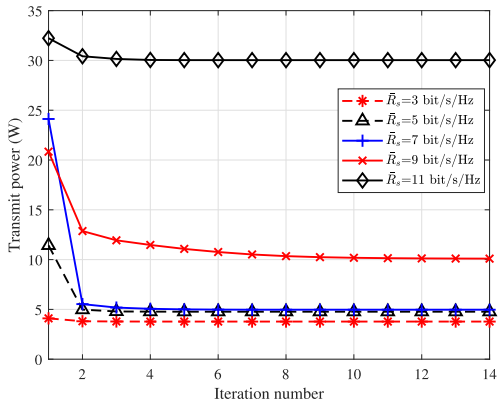

Fig. 6. Transmit power vs. Iteration number for SDMA transmission scheme, $K = 2, M = 3, M_2 = 2, \bar{R}_c = 0.5$ bit/s/Hz.

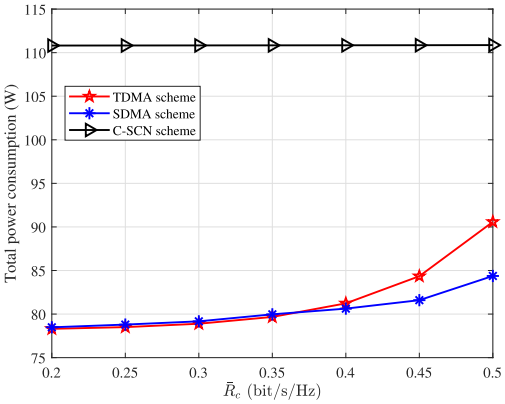

Fig. 7. Total power consumption vs. $\bar{R}_c$, $K = 2, M = 3, M_2 = 2$.

Next, the total power consumption versus the micro user's minimum transmission rate requirement $\bar{R}_c$ is plotted for different schemes with $K = 2, M = 3$ in Fig. 7 and $K = 3, M = 4$ in Fig. 8. As shown in these figures, the total power consumption increases as $\bar{R}_c$ increases for the SDMA scheme and TDMA scheme. When $\bar{R}_c$ is low, for example, $\bar{R}_c \leq 0.3$ bit/s/Hz, the TDMA scheme is slightly better than the SDMA scheme, but the performance gap is negligible. When $\bar{R}_c$ is high, the SDMA scheme presents

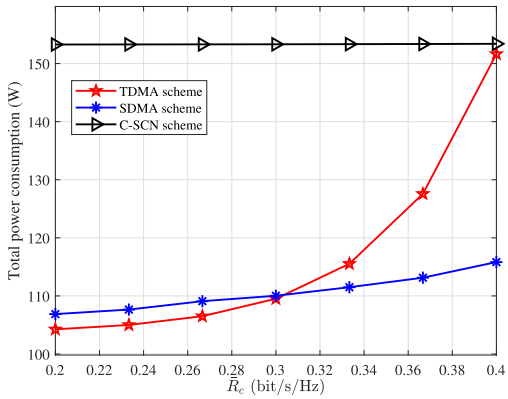

Fig. 8. Total power consumption vs. $\bar{R}_c$, $K = 3, M = 4, M_2 = 3$.

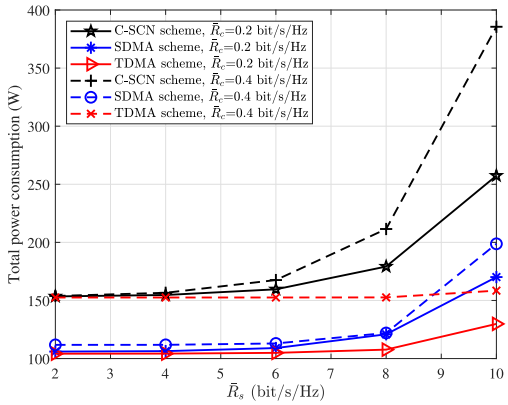

Fig. 9. Total power consumption vs. $\bar{R}_s$, $K = 3, M = 4, M_2 = 3$.

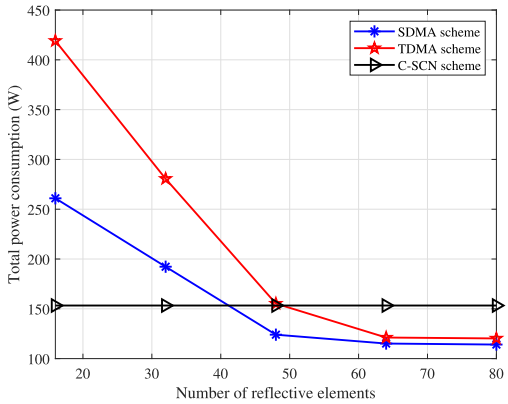

Fig. 10. Total power consumption vs. Number of reflective elements, $K = 3, M = 4, M_2 = 3, \bar{R}_c = 0.35$ bit/s/Hz.

much better performance over the TDMA scheme. Hence, when the rate requirement of micro users is not stringent, we choose the TDMA transmission scheme to serve the micro users one by one, while SDMA is preferable when the requirement is strict. In addition, the proposed TDMA and SDMA schemes significantly outperform the C-SCN scheme. By employing the RIS in the SCN to serve multiple micro users, the total power consumption of the RIS-based SCN becomes drastically lower than the conventional SCN. For instance, when $\bar{R}_c = 0.5$ bit/s/Hz, the power consumption of the SDMA scheme, TDMA scheme, and C-SCN scheme are 84.37 W, 90.58 W, and 110.9 W, respectively. With $K = 2$, the reduction ranges of total power consumption in the SDMA scheme and TDMA scheme are 24 percent to 29 percent and 18 percent to 29 percent, respectively, compared to the C-SCN scheme. With $K = 3$, the reduction ranges are 25 percent to 30 percent and 1 percent to 32 percent. These results verify that introducing the RIS into the SCN to serve multiple micro users is a promising technique to reduce the total power consumption and realize more energy-efficient communication. Furthermore, comparing Fig. 7 and Fig. 8, we observe that the total power consumption of the TDMA scheme with three micro users increases faster than that of the TDMA scheme with two micro users. This can be explained as follows. The transmission rate requirement of each micro user under the TDMA scheme is scaled up by K due to the reduction in transmission time. A larger K value will lead to a more stringent rate requirement for micro users under the TDMA scheme. In contrast, the performance of the SDMA scheme is not affected by K as much as the TDMA scheme.

In Fig. 9, we study the impact of the macro user rate requirement $\bar{R}_s$ on the performance of different transmission schemes. It is seen from this figure that the total power consumption achieved by all the transmission schemes increases as $\bar{R}_s$ increases, because more power is required to support faster data transmission. In addition, for the three transmission schemes, a higher $\bar{R}_c$ calls for higher total power consumption. Again, the TDMA scheme and SDMA scheme both outperform the C-SCN scheme. We also observe that the total power consumption of the C-SCN scheme increases more rapidly than those of the TDMA and SDMA schemes.

Fig. 10 plots the total power consumption versus the number of reflective elements. As expected, with the increase in the number of reflective elements, the total power consumption of the proposed scheme decreases since a larger degree of freedom can be utilized to optimize the system. When N is not large, for instance, $N = 16$, the power saving benefit by deploying the RIS cannot be ensured. When N is larger than 48, the total power consumption of the proposed RIS-based SCN is lower than that of the conventional SCN, which shows the benefit in power saving by deploying the RIS instead of an mBS. Meanwhile, the total power consumption approaches a constant value when N is sufficiently large.

VI. Conclusion

In this paper, we have proposed a novel RIS-based SCN by replacing the mBS in the SCNs with the RIS. Compared with deploying mBSs, the proposed system can achieve higher energy efficiency since the RIS transmits messages by reflecting the incident signal passively. The interference challenge faced by the conventional SCN can also be solved since the interference relationship is transformed to a mutualistic one. The SDMA and TDMA transmission schemes have been developed to support multi-user information transmission. A joint beamforming and phase shifts design problem has been formulated to minimize the total power consumption under the user transmission rate and phase shift constraints. For the

two problems under SDMA and TDMA transmission schemes, alternating optimization algorithms have been proposed to solve two subproblems iteratively, one to optimize the phase shifts and the other to optimize the beamforming vector. Simulation results have shown that the power consumption can be reduced significantly by deploying the RIS, which validates the advantages of the RIS-based SCN and the effectiveness of the proposed algorithms.

REFERENCES

[1] J. Wang, Y.-C. Liang, Y. Pei, and X. S. Shen, "Reconfigurable intelligent surface for small cell network," in *Proc. IEEE Global Commun. Conf. (GLOBECOM)*, Madrid, Spain, Dec. 2021, pp. 1–6.

[2] F. Tariq, M. R. A. Khandaker, K.-K. Wong, M. A. Imran, M. Bennis, and M. Debbah, "A speculative study on 6G," *IEEE Wireless Commun.*, vol. 27, no. 4, pp. 118–125, Aug. 2020.

[3] X. Ge, J. Yang, H. Gharavi, and Y. Sun, "Energy efficiency challenges of 5G small cell networks," *IEEE Commun. Mag.*, vol. 55, no. 5, pp. 184–191, May 2017.

[4] H. Claussen, D. Lopez-Perez, L. Ho, R. Razavi, and S. Kucera, *Small Cell Networks: Deployment, Management, and Optimization*. Hoboken, NJ, USA: Wiley, 2017.

[5] S. M. Cheng, S. Y. Lien, F. S. Chu, and K. C. Chen, "On exploiting cognitive radio to mitigate interference in macro/femto heterogeneous networks," *IEEE Wireless Commun.*, vol. 18, no. 3, pp. 40–47, Jun. 2011.

[6] H. Zhang, Y. Wang, and H. Ji, "Resource optimization-based interference management for hybrid self-organized small-cell network," *IEEE Trans. Veh. Technol.*, vol. 65, no. 2, pp. 936–946, Feb. 2015.

[7] Z. Zhang, L. Song, Z. Han, and W. Saad, "Coalitional games with overlapping coalitions for interference management in small cell networks," *IEEE Trans. Wireless Commun.*, vol. 13, no. 5, pp. 2659–2669, May 2014.

[8] A. Liu, V. K. N. Lau, L. Ruan, J. Chen, and D. Xiao, "Hierarchical radio resource optimization for heterogeneous networks with enhanced inter-cell interference coordination (eICIC)," *IEEE Trans. Signal Process.*, vol. 62, no. 7, pp. 1684–1693, Apr. 2014.

[9] D. Lopez-Perez, A. Valcarce, G. De La Roche, and J. Zhang, "OFDMA femtocells: A roadmap on interference avoidance," *IEEE Commun. Mag.*, vol. 47, no. 9, pp. 41–48, Sep. 2009.

[10] N. Saquib, E. Hossain, and D. I. Kim, "Fractional frequency reuse for interference management in LTE-advanced hetnets," *IEEE Wireless Commun.*, vol. 20, no. 2, pp. 113–122, Apr. 2013.

[11] W. Shin, W. Noh, K. Jang, and H.-H. Choi, "Hierarchical interference alignment for downlink heterogeneous networks," *IEEE Trans. Wireless Commun.*, vol. 11, no. 12, pp. 4549–4559, Dec. 2012.

[12] L. Liu, J. C. Zhang, Y. Yi, H. Li, and J. Zhang, "Combating interference: Mu-MIMO CoMP and HetNet," *J. Commun.*, vol. 7, no. 9, pp. 646–655, 2012.

[13] V. Chandrasekhar, J. G. Andrews, T. Muharemovic, Z. Shen, and A. Gatherer, "Power control in two-tier femtocell networks," *IEEE Trans. Wireless Commun.*, vol. 8, no. 8, pp. 4316–4328, Aug. 2009.

[14] J. Xiao, C. Yang, A. Anpalagan, Q. Ni, and M. Guizani, "Joint interference management in ultra-dense small-cell networks: A multi-domain coordination perspective," *IEEE Trans. Commun.*, vol. 66, no. 11, pp. 5470–5481, Nov. 2018.

[15] W. Guo and T. O'Farrell, "Green cellular network: Deployment solutions, sensitivity and tradeoffs," in *Proc. Wireless Adv.*, Jun. 2011, pp. 42–47.

[16] R. Tao, W. Liu, X. Chu, and J. Zhang, "An energy saving small cell sleeping mechanism with cell range expansion in heterogeneous networks," *IEEE Trans. Wireless Commun.*, vol. 18, no. 5, pp. 2451–2463, May 2019.

[17] J. A. Ayala-Romero, J. J. Alcaraz, A. Zanella, and M. Zorzi, "Online learning for energy saving and interference coordination in HetNets," *IEEE J. Sel. Areas Commun.*, vol. 37, no. 6, pp. 1374–1388, Jun. 2019.

[18] L. Tang, W. Wang, Y. Wang, and Q. Chen, "An energy-saving algorithm with joint user association, clustering, and on/off strategies in dense heterogeneous networks," *IEEE Access*, vol. 5, pp. 12988–13000, 2017.

[19] C. Liaskos, S. Nie, A. Tsioliaridou, A. Pitsillides, S. Ioannidis, and I. Akyildiz, "A new wireless communication paradigm through software-controlled metasurfaces," *IEEE Commun. Mag.*, vol. 56, no. 9, pp. 162–169, Sep. 2018.

[20] Q. Wu and R. Zhang, "Intelligent reflecting surface enhanced wireless network via joint active and passive beamforming," *IEEE Trans. Wireless Commun.*, vol. 18, no. 11, pp. 5394–5409, Nov. 2019.

[21] S. Zeng, H. Zhang, B. Di, Z. Han, and L. Song, "Reconfigurable intelligent surface (RIS) assisted wireless coverage extension: RIS orientation and location optimization," *IEEE Commun. Lett.*, vol. 25, no. 1, pp. 269–273, Jan. 2020.

[22] P. Wang, J. Fang, X. Yuan, Z. Chen, and H. Li, "Intelligent reflecting surface-assisted millimeter wave communications: Joint active and passive precoding design," *IEEE Trans. Veh. Technol.*, vol. 69, no. 12, pp. 14960–14973, Oct. 2020.

[23] Y.-C. Liang, R. Long, Q. Zhang, J. Chen, H. V. Cheng, and H. Guo, "Large intelligent surface/antennas (LISA): Making reflective radios smart," *J. Commun. Inf. Netw.*, vol. 4, no. 2, pp. 40–50, Jun. 2019.

[24] J. Wang, Y.-C. Liang, J. Joung, X. Yuan, and X. Wang, "Joint beamforming and reconfigurable intelligent surface design for two-way relay networks," *IEEE Trans. Commun.*, vol. 69, no. 8, pp. 5620–5633, Aug. 2021.

[25] M. Jung, W. Saad, and G. Kong, "Performance analysis of active large intelligent surfaces (LISs): Uplink spectral efficiency and pilot training," *IEEE Trans. Commun.*, vol. 69, no. 5, pp. 3379–3394, May 2021.

[26] Z. Li, H. Hu, J. Zhang, and J. Zhang, "Enhancing indoor mmWave wireless coverage: Small-cell densification or reconfigurable intelligent surfaces deployment?" *IEEE Wireless Commun. Lett.*, vol. 10, no. 11, pp. 2547–2551, Nov. 2021.

[27] A. Bereyhi, V. Jamali, R. R. Müller, A. M. Tulino, G. Fischer, and R. Schober, "A single-RF architecture for multiuser massive MIMO via reflecting surfaces," in *Proc. IEEE Int. Conf. Acoust., Speech Signal Process. (ICASSP)*, May 2020, pp. 8688–8692.

[28] W. Tang *et al.*, "Wireless communications with programmable metasurface: Transceiver design and experimental results," *China Commun.*, vol. 16, no. 5, pp. 46–61, May 2019.

[29] Q. Zhang, Y.-C. Liang, and H. V. Poor, "Reconfigurable intelligent surface assisted MIMO symbiotic radio networks," *IEEE Trans. Commun.*, vol. 69, no. 7, pp. 4832–4846, Jul. 2021, doi: 10.1109/TCOMM.2021.3070043.

[30] J. Hu, Y.-C. Liang, and Y. Pei, "Reconfigurable intelligent surface enhanced multi-user MISO symbiotic radio system," *IEEE Trans. Commun.*, vol. 69, no. 4, pp. 2359–2371, Dec. 2021.

[31] M. Hua, L. Yang, Q. Wu, C. Pan, C. Li, and A. L. Swindlehurst, "UAV-assisted intelligent reflecting surface symbiotic radio system," *IEEE Trans. Wireless Commun.*, vol. 20, no. 9, pp. 5769–5785, Sep. 2021.

[32] L. Zhang *et al.*, "A wireless communication scheme based on space- and frequency-division multiplexing using digital metasurfaces," *Nature Electron.*, vol. 4, no. 3, pp. 218–227, Mar. 2021.

[33] Y.-C. Liang, Q. Zhang, E. G. Larsson, and G. Y. Li, "Symbiotic radio: Cognitive backscattering communications for future wireless networks," *IEEE Trans. Cognit. Commun. Netw.*, vol. 6, no. 4, pp. 1242–1255, Sep. 2020.

[34] Q. Nadeem, A. Kammoun, A. Chaaban, M. Debbah, and M.-S. Alouini, "Asymptotic max-min SINR analysis of reconfigurable intelligent surface assisted MISO systems," *IEEE Trans. Wireless Commun.*, vol. 19, no. 12, pp. 7748–7764, Dec. 2020.

[35] C. Hu, L. Dai, S. Han, and X. Wang, "Two-timescale channel estimation for reconfigurable intelligent surface aided wireless communications," *IEEE Trans. Commun.*, vol. 69, no. 11, pp. 7736–7747, Nov. 2021.

[36] A. L. Swindlehurst, G. Zhou, R. Liu, C. Pan, and M. Li, "Channel estimation with reconfigurable intelligent surfaces—A general framework," *Proc. IEEE*, vol. 110, no. 9, pp. 1312–1338, Sep. 2022.

[37] B. Zheng, C. You, W. Mei, and R. Zhang, "A survey on channel estimation and practical passive beamforming design for intelligent reflecting surface aided wireless communications," *IEEE Commun. Surveys Tuts.*, vol. 24, no. 2, pp. 1035–1071, 2nd Quart., 2022.

[38] J. Chen, Y.-C. Liang, H. V. Cheng, and W. Yu, "Channel estimation for reconfigurable intelligent surface aided multi-user MIMO systems," 2019, *arXiv:1912.03619*.

[39] G. Yang, Q. Zhang, and Y.-C. Liang, "Cooperative ambient backscatter communications for green Internet-of-Things," *IEEE Internet Things J.*, vol. 5, no. 2, pp. 1116–1130, Apr. 2018.

[40] W. Liu, S. Han, C. Yang, and C. Sun, "Massive MIMO or small cell network: Who is more energy efficient?" in *Proc. IEEE Wireless Commun. Netw. Conf. Workshops (WCNCW)*, Shanghai, China, Apr. 2013, pp. 24–29.

[41] C. Huang, A. Zappone, G. C. Alexandropoulos, M. Debbah, and C. Yuen, "Reconfigurable intelligent surfaces for energy efficiency in wireless communication," *IEEE Trans. Wireless Commun.*, vol. 18, no. 8, pp. 4157–4170, Aug. 2019.
[42] S. Abeywickrama, R. Zhang, Q. Wu, and C. Yuen, "Intelligent reflecting surface: Practical phase shift model and beamforming optimization," *IEEE Trans. Commun.*, vol. 68, no. 9, pp. 5849–5863, Sep. 2020.
[43] W. Cai, H. Li, M. Li, and Q. Liu, "Practical modeling and beamforming for intelligent reflecting surface aided wideband systems," *IEEE Commun. Lett.*, vol. 24, no. 7, pp. 1568–1571, Jul. 2020.
[44] M. Grant and S. Boyd. (Jan. 2020). *CVX: MATLAB software for disciplined convex programming, version 2.2*. [Online]. Available: http://cvxr.com/cvx
[45] Z.-Q. Luo, W.-K. Ma, A. M.-C. So, Y. Ye, and S. Zhang, "Semidefinite relaxation of quadratic optimization problems," *IEEE Signal Process. Mag.*, vol. 27, no. 3, pp. 20–34, May 2010.
[46] A. A. Nasir, H. D. Tuan, T. Q. Duong, and H. V. Poor, "Secrecy rate beamforming for multicell networks with information and energy harvesting," *IEEE Trans. Signal Process.*, vol. 65, no. 3, pp. 677–689, Feb. 2016.
[47] B. R. Marks and G. P. Wright, "A general inner approximation algorithm for nonconvex mathematical programs," *Oper. Res.*, vol. 26, pp. 681–683, Jul. 1978.

Jun Wang (Graduate Student Member, IEEE) received the B.S. degree in communication engineering from the University of Electronic Science and Technology of China (UESTC), Chengdu, China, in 2018, where he is currently pursuing the Ph.D. degree with the National Key Laboratory of Science and Technology on Communications. His research interests include symbiotic radio, reconfigurable intelligent surface, and convex optimization.

Ying-Chang Liang (Fellow, IEEE) was a Professor with The University of Sydney, Sydney, NSW, Australia, a Principal Scientist and a Technical Advisor with the Institute for Infocomm Research, Singapore, and a Visiting Scholar with Stanford University, Stanford, CA, USA. He is currently a Professor with the University of Electronic Science and Technology of China, Chengdu, China, where he leads the Center for Intelligent Networking and Communications (CINC). His research interests include wireless networking and communications, cognitive radio, symbiotic communications, dynamic spectrum access, the Internet of Things, artificial intelligence, and machine learning techniques.

He is a Foreign Member of the Academia Europaea. He received the Prestigious Engineering Achievement Award from The Institution of Engineers, Singapore, in 2007; the Outstanding Contribution Appreciation Award from the IEEE Standards Association in 2011; and the Recognition Award from the IEEE Communications Society Technical Committee on Cognitive Networks in 2018. He was a recipient of numerous paper awards, including the IEEE Communications Society Advances in Communication Prize Paper Award in 2022, the IEEE Communications Society Stephen O. Rice Prize in 2021, and the IEEE Vehicular Technology Society Jack Neubauer Memorial Award in 2014. He was the Chair of the IEEE Communications Society Technical Committee on Cognitive Networks. He has served as the TPC Chair and the Executive Co-Chair for the IEEE Globecom'17. He was a Guest/Associate Editor of the IEEE TRANSACTIONS ON WIRELESS COMMUNICATIONS, the IEEE JOURNAL ON SELECTED AREAS IN COMMUNICATIONS, the *IEEE Signal Processing Magazine*, the IEEE TRANSACTIONS ON VEHICULAR TECHNOLOGY, and the IEEE TRANSACTIONS ON SIGNAL AND INFORMATION PROCESSING OVER NETWORKS, and an Associate Editor-in-Chief of the *Random Matrices: Theory and Applications* (World Scientific). He is also the Founding Editor-in-Chief of the IEEE JOURNAL ON SELECTED AREAS IN COMMUNICATIONS: COGNITIVE RADIO SERIES and the Key Founder and the Editor-in-Chief of the IEEE TRANSACTIONS ON COGNITIVE COMMUNICATIONS AND NETWORKING. He is also serving as an Associate Editor-in-Chief for China Communications. He was a Distinguished Lecturer of the IEEE Communications Society and the IEEE Vehicular Technology Society. He has been recognized by Thomson Reuters (now Clarivate Analytics) as a Highly Cited Researcher since 2014.

Yiyang Pei (Senior Member, IEEE) received the B.Eng. and Ph.D. degrees in electrical and electronic engineering from Nanyang Technological University, Singapore, in 2007 and 2012, respectively. From 2012 to 2016, she was a Research Scientist with the Institute for Infocomm Research, Singapore. She is currently an Associate Professor with the Singapore Institute of Technology, Singapore. Her current research interests include reconfigurable intelligent surface, dynamic spectrum access, and application of machine learning to wireless communications and networks. She was a recipient of the IEEE Communications Society Stephen O. Rice Prize Paper Award in 2021. She is an Editor of the IEEE TRANSACTIONS ON COGNITIVE COMMUNICATIONS AND NETWORKING.

Xuemin (Sherman) Shen (Fellow, IEEE) received the Ph.D. degree in electrical engineering from Rutgers University, New Brunswick, NJ, USA, in 1990.

He is currently a University Professor with the Department of Electrical and Computer Engineering, University of Waterloo, Canada. His research interests include network resource management, wireless network security, the Internet of Things, 5G and beyond, and vehicular networks. He is a registered Professional Engineer of Ontario, Canada, an Engineering Institute of Canada Fellow, a Canadian Academy of Engineering Fellow, a Royal Society of Canada Fellow, a Chinese Academy of Engineering Foreign Member, and a Distinguished Lecturer of the IEEE Vehicular Technology Society and Communications Society. He received the Canadian Award for Telecommunications Research from the Canadian Society of Information Theory (CSIT) in 2021; the R.A. Fessenden Award from IEEE, Canada, in 2019; the Award of Merit from the Federation of Chinese Canadian Professionals (Ontario) in 2019; the James Evans Avant Garde Award from the IEEE Vehicular Technology Society in 2018; the Joseph LoCicero Award in 2015; the Education Award from the IEEE Communications Society (ComSoc) in 2017; and the Technical Recognition Award from the Wireless Communications Technical Committee in 2019 and the AHSN Technical Committee in 2013. He has also received the Excellent Graduate Supervision Award in 2006 from the University of Waterloo and the Premier's Research Excellence Award (PREA) from the Province of Ontario, Canada, in 2003. He has served as the Technical Program Committee Chair/Co-Chair for IEEE Globecom'16, IEEE Infocom'14, IEEE VTC'10 Fall, and IEEE Globecom'07, and the Chair for the IEEE ComSoc Technical Committee on Wireless Communications. He is the President of the IEEE ComSoc. He was the Vice President of Technical and Educational Activities and the Publications. He was a Member-at-Large on the Board of Governors, the Chair of the Distinguished Lecturer Selection Committee, and a member of IEEE Fellow Selection Committee of the ComSoc. He served as the Editor-in-Chief of the IEEE INTERNET OF THINGS JOURNAL, IEEE NETWORK, and *IET Communications*.